JOURNAL OF GEOPHYSICAL RESEARCH, VOL. 112, F04010, doi:10.1029/2006JF000729, 2007

Relation between rock uplift and denudation from cosmogenic nuclides in river sediment in the Central Alps of Switzerland

Hella Wittmann,[1] Friedhelm von Blanckenburg,[1] Tina Kruesmann,[1,2] Kevin P. Norton,[1] and Peter W. Kubik[3]

Received 6 December 2006; revised 25 June 2007; accepted 3 August 2007; published 29 November 2007.

[1] A north-south traverse through the Swiss Central Alps reveals that denudation rates correlate with recent rock uplift rates in both magnitude and spatial distribution. This result emerges from a study of in situ–produced cosmogenic ^{10}Be in riverborne quartz in Central Alpine catchments. As a prerequisite, we took care to investigate the potential influence of shielding from cosmic rays due to snow, glaciers, and topographic obstructions; to calculate a possible memory from Last Glacial Maximum (LGM) glaciation; and to identify a watershed size that is appropriate for systematic sampling. Mean denudation rates are 0.27 ± 0.14 mm/a for the Alpine foreland and 0.9 ± 0.3 mm/a for the crystalline Central Alps. The measured cosmogenic nuclide-derived denudation rates are in good agreement with post-LGM lake infill rates and are about twice as high as denudation rates from apatite fission track ages that record denudation from 9 to 5 Ma. In general, denudation rates are high in areas of high topography and high crustal thickness. The similarity in the spatial distribution and magnitude of denudation rates and those of rock uplift rates can be interpreted in several ways: (1) Postglacial rebound or climate change has introduced a transient change in which both uplift and denudation follow each other with a short lag time; (2) the amplitude of glacial to interglacial changes in both is small and is contained in the scatter of the data; (3) both are driven by ongoing convergence where their similarity might hint at some form of long-term quasi steady state; or (4) enhanced continuous Quaternary erosion and isostatic compensation of the mass removed accounts for the distribution of present-day rock uplift.

Citation: Wittmann, H., F. von Blanckenburg, T. Kruesmann, K. P. Norton, and P. W. Kubik (2007), Relation between rock uplift and denudation from cosmogenic nuclides in river sediment in the Central Alps of Switzerland, *J. Geophys. Res.*, *112*, F04010, doi:10.1029/2006JF000729.

1. Introduction

[2] In convergent mountain belts with thickened crust, relief forms when the uplift rate exceeds the denudation rate. Once a certain topography that is characteristic of convergence rate, orogen width, crustal thickness, rock strength, and denudational power (set by climate) is achieved, any further rock uplift will be balanced by denudation. Steady state between rock uplift and denudation is established and the characteristic relief will be maintained. These concepts have been detailed in theory [*England and Molnar*, 1990; *Stuewe and Barr*, 1998; *Whipple et al.*, 1999; *Whipple*, 2001, 2004; *Willett and Brandon*, 2002] and documented with field data from various mountain belts [*Koons*, 1989; *Brandon and Vance*, 1992; *Small et al.*, 1997; *Hovius et al.*, 2000; *Montgomery and Greenberg*, 2000; *Kuhlemann et al.*, 2002; *Montgomery and Brandon*, 2002].

[3] The significance of these concepts remains disputed because field tests are not sufficiently comprehensive to allow for a self-consistent characterization of the responses to forcing. Further they suffer from the need to bridge the substantial methodological timescales [*Hovius and von Blanckenburg*, 2007]; rock uplift can be measured with geodetic methods relative to a fixed datum on preserved surfaces (10^1 a timescale), while the integrated result of uplift can be determined by stable isotope-based paleoaltimetry (10^6 a) [*Mulch et al.*, 2007]. Denudation can be measured by river loads (10^1 a) [*Pinet and Souriau*, 1988; *Summerfield and Hulton*, 1994], sediment budgets (e.g., lake fills; 10^4 to 10^6 a), and thermochronology (10^6 a).

[4] Cosmogenic nuclides in river sediment potentially provide a denudation rate tool that is suitable to bridge these timescales. The measured rates integrate over a timescale (10^2 to 10^4 a) that is sufficiently long to be insensitive to very short-term denudational perturbations (human influence, short-term climate oscillations), and that

[1] Institut für Mineralogie, Universität Hannover, Hannover, Germany.
[2] Now at GeoForschungsZentrum Potsdam, Telegrafenberg, Potsdam, Germany.
[3] Paul Scherrer Institut and Institute of Particle Physics, ETH Zurich, Zurich, Switzerland.

0148-0227/07/2006JF000729$09.00

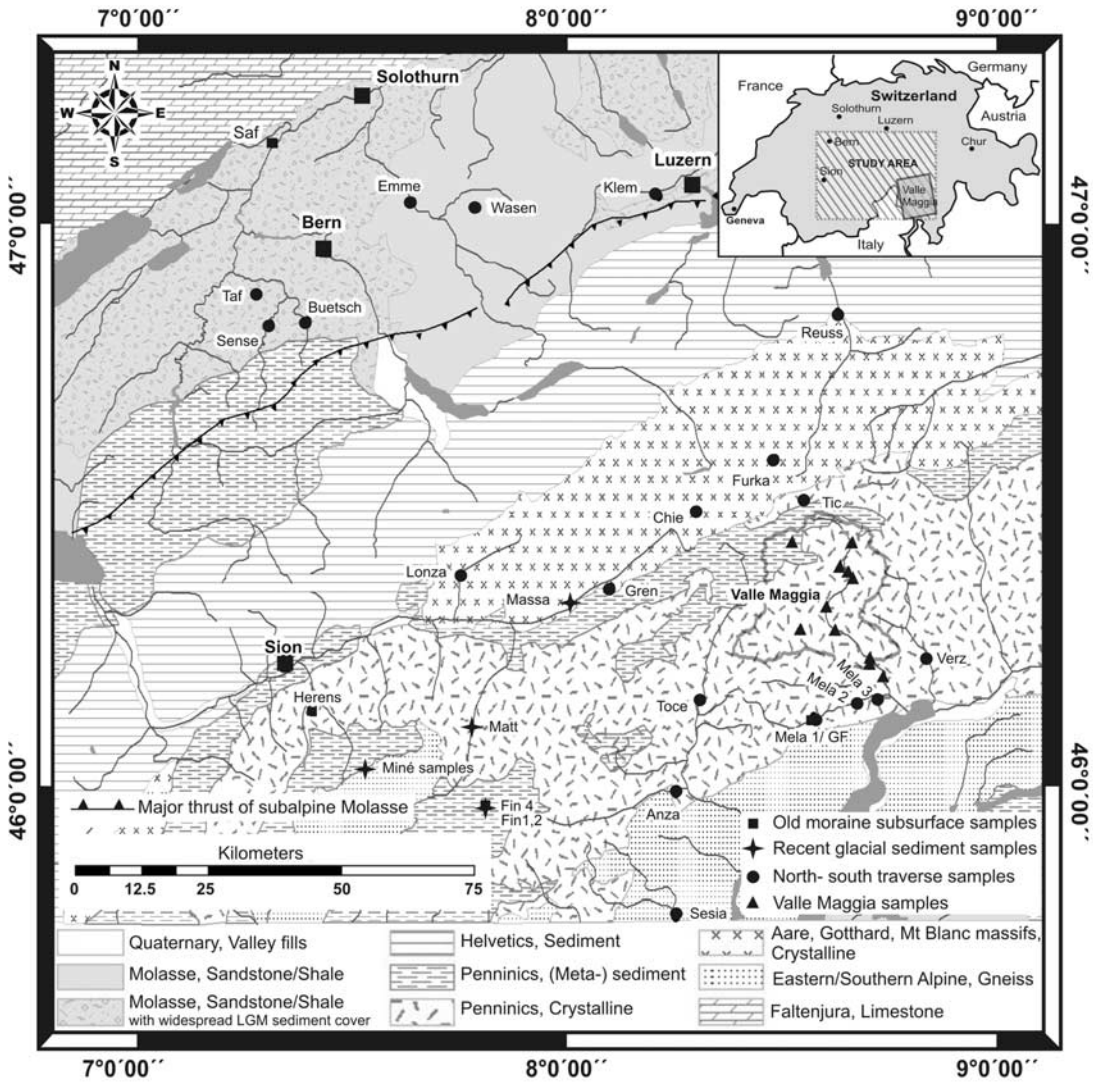

Figure 1. Geological overview over the sampling area and sampling locations. Shown are old moraine subsurface samples (squares), recent glacial sediment samples (stars), north-south traverse samples (circles), and samples within the Maggia catchment (Valle Maggia, triangles).

is meaningful for timescales of both rock weathering and rock uplift [*von Blanckenburg*, 2005].

[5] Here, we apply this technique to the European Alps. The Alps, and in particular the Swiss Central Alps, are an area of exceptionally high density and quality of geologic data. The collision history is well known [*Schmid and Kissling*, 2000; *Schmid et al.*, 2004], long-term denudation rates are known from thermochronological studies [*Wagner et al.*, 1977; *Rahn*, 2001, 2005], and present-day geodetic rock uplift rates have been determined (*Kahle et al.* [1997], revised by *Schlatter et al.* [2005]). In addition the spatial and temporal distribution of ice cover during the Last Glacial Maximum (LGM), and postglacial periods is well constrained [*Florineth and Schluechter*, 1998; *Ivy-Ochs et al.*, 2004; *Kelly et al.*, 2004].

[6] However, since a systematic investigation of the applicability of cosmogenic nuclides to active, rapidly denuding mountain belts with all their complexities has not yet been done, we first establish the sensitivity of the method to certain potential perturbations. These are (1) the approach of nuclide concentrations to steady state after LGM glaciation, (2) the nuclide inventory of potentially incorporated moraine and glacial material, and (3) watershed sizes that are too small or too large for representative sampling.

[7] Following the establishment of these prerequisites, we proceed to map a first-order north-south traverse of denudation rates across the orogen. We will show that these relate to topography and rock uplift rates. Finally, we will discuss possible controlling factors and feedback mechanisms.

2. Study Area, Sample Characteristics, and Lab Processing

2.1. Tectonic Evolution of the Alps and Alpine Glacial History

[8] Our study area comprises the Swiss Mittelland, the Swiss Central Alps, and the Italian section of the Central Alps (see Figure 1 and Table 1). In this study, the latter two are called the "high Alps." Continental convergence and

Table 1. Sample Specific and Basin Characteristics

Sample Type	Sample Name	Catchment	Grain Size Fraction, μm	Sample Altitude,[a] m	Position on Swiss Map,[b] m		Drainage Area, km^2	Mean Altitude, m	Mean Slope of Catchment, %
					E	N			
LGM or younger moraine samples	Saf 1-1	Aare, gravel Pit "Biedermann"	400–1000	430	592000	224000	7868	1158	14
	Saf 1-2	(Replicate of Saf 1-1)	400–1000	430	592000	224000	7868	1158	14
	Herens	Borgne	400–1000	1100	599000	112000	236	2536	26
	Fin 4	Findeland Glacier	400–1000	2500	629500	95000	12	3272	14
	Mela 1 GF	Melezza, Centovalli at Dissimo	125–250	625	688430	112050	106	2959	24
Recent glacial sediment samples	Fin 1	Findeland Glacier: shear plane	400–1000	2960	629300	95500	4	3174	21
	Fin 2	Findeland Glacier: glacier mouth	400–1000	2550	629200	95300	30	3168	18
	Miné 4-1	Mount Miné Glacier: southern mouth	400–1000	1980	609000	100000	49	2959	24
	Miné 4-2	(Replicate of Miné 4-1)	400–1000	1980	609000	100000	49	2959	24
	Miné 5	Mount Miné Glacier: northern mouth	400–1000	1980	609000	100000	49	2959	24
	Miné 6	Mount Miné Glacier: lateral moraine	400–1000	1980	609000	100000	49	2959	24
	Massa	Massa, northern Valais	400–1000	800	644000	132000	201	2889	22
	Matt	Mattervispa, southern Valais	400–1000	1525	626000	105000	326	2902	24
Maggia sediment samples	Mag 1	Maggia, Val di Gei	500–800	310	700410	119560	11	1434	30
	Mag 2	Maggia, Val del Salto	500–800	332	698040	122860	20	1439	31
	Mag 4	Rovana, Valle di Campo	500–800	780	686000	129410	67	1826	30
	Mag 8	Bavona, Val Bavona	500–800	443	690430	133390	119	1930	30
	Mag 10	Maggia, Val di Prato	500–800	715	695120	138650	31	2011	31
	Mag 11-2	Maggia, Val di Maggia at Riveo	500–800	391	691930	128780	452	1818	29
	Mag 11-4	Maggia, Val di Maggia at Moghegno	500–800	314	698980	122930	544	1726	29
	Mag 13	Maggia, Lago Bianco and Lago Nero	800–1000	1984	684020	145220	10	2522	27
	Mag 16	Maggia, Val Lavizzara and Val di Peccia	500–800	740	693880	139810	88	1966	28
	Mag 17	Maggia, Val di Peccia	500–800	880	692120	141600	46	1971	28
	Mag 18	Maggia, side valley of Val Lavizzara	500–800	1260	694350	145370	7	2138	27
North-south traverse samples	Anza	Anza, Valle Anzasca	125–250	248	663540	97230	259	1782	31
	Sesia	Sesia, Valle delle Sesia	125–250	428	664720	73370	626	1589	29
	Toce a	Toce, Valle Antigorio	250–500	346	668720	115200	361	1940	27
	Toce b	Toce, Valle Antigorio	800–1000	346	668720	115200	361	1940	27
	Verz a	Verzasca, Valle Verzasca	500–800	519	708830	123470	186	1671	30
	Verz b	Verzasca, Valle Verzasca	800–1000	519	708830	123470	186	1671	30
	Mela 1	Melezza, Centovalli at Dissimo	125–250	625	688430	112050	106	1349	24
	Mela 2	Melezza, Centovalli at Intragna	125–250	260	698070	115910	166	1229	24
	Mela 3a	Melezza, Centovalli at Verscio	125–250	245	698580	116040	333	1340	27
	Mela 3b	Melezza, Centovalli at Verscio	250–500	245	698580	116040	333	1340	27
	Lonza	Lonza, northern Valais	400–1000	1376	627000	138000	99	2551	28
	Gren	Milibach, southern Valais	400–1000	1037	651000	136000	6	1988	29
	Chie	Chietalbach, Chietal	500–800	1344	667500	151040	156	2368	24
	Furka	Furkareuss, Furkatal	250–1000	1637	681420	160470	29	2486	23
	Tic a	Ticino, Val Bedretto	125–250	1254	686130	152720	78	2169	25
	Tic b	Ticino, Val Bedretto	250–500	1254	686130	152720	78	2169	25
	Reuss a	Reuss, Reuss- Valley	125–250	453	707940	165830	683	2095	28
	Reuss b	Reuss, Reuss- Valley	250–500	453	707940	165830	683	2095	28
	Klem a	Kleine Emme, Emmental	125–250	470	659500	211480	434	1088	16
	Klem b	Kleine Emme, Emmental	250–500	470	659500	211480	434	1088	16
	Buetsch 1	Bütschelbach, Mittelland (ng)	400–1000	742	599200	188200	12	885	9
	Buetsch 2	Bütschelbach, Mittelland (ng)	400–1000	742	600600	187200	8	885	9
	Emme	Emme, Mittelland	400–1000	600	615000	209000	675	981	13
	Wasen 1-1	Liechtguetbach, Mittelland	400–1000	775	628000	208000	12	1047	16
	Wasen 1-2	(replicate of Wasen 1-1)	400–1000	775	628000	208000	12	1047	16
	Taf	Tafersbach, Mittelland	400–1000	560	589000	191700	25	692	5
	Sense	Sense, Mittelland	400–1000	547	591000	186000	162	1292	16

[a]Taken from Carte Nationale de la Suisse.
[b]Based on Swiss grid coordinate system; reference frame is CH 1903; (ng) is Mittelland catchment that was not covered by LGM glaciers.

collision of the Adriatic microplate and the European continent at 55 Ma initiated the formation of the Alpine orogen [*Schmid and Kissling*, 2000]. The European Alps feature a crystalline core comprising polymetamorphic rocks and pre-Alpine magmatic rocks overlain by Mesozoic and Cenozoic metasedimentary sequences, which both form the Penninic and Helvetic thrust nappes. Between the Alps to the south and the Jura fold-and-thrust belt to the north, the Swiss Mittelland forms a foreland basin, containing Tertiary molasse sediments with a minimum age of ~5 Ma. In the south of the Central Alps, the Tonale Line, an E-W striking segment of the Insubric Line separates the Southern Alps from the Central Alps. The Southern Alps contain crystalline (magmatic and metamorphic) rocks dated at 300 to 200 Ma and Mesozoic sedimentary sequences. The Insubric Line, a presently inactive fault zone [*Prosser*, 1998; *Schmid et al.*, 2004] was active from Oligocene to early Miocene times, marking the position of the Adriatic indenter tip during the formation of the Alpine orogen [*Schmid et al.*, 1989].

[9] During the LGM, glaciers extended from the large ice domes in the Alpine core to the foreland basins [*Florineth and Schluechter*, 1998, 2000; *Kelly et al.*, 2004]. During this time, as much as 60% of the Mittelland basin was covered by ice. Beginning at 21 ka, the piedmont glaciers that occupied the Mittelland rapidly retreated into the Central Alpine valleys [*Ivy-Ochs et al.*, 2004], leaving the foreland basins ice free. Alpine glaciers never grew large enough during any of the subsequent advances to cover the foreland again. Glaciers continued however to impact the Central Alps. Numerous Late Glacial stadials have been identified in the Alps. Immediately after LGM deglaciation, small fluctuations (Bühl and Steinach advances) were followed by the larger Gschnitz, Clavadel-Senders, and Daun Stadials [*van Husen*, 1977; *Maisch*, 1981; *Ivy-Ochs et al.*, 2004]. These colder periods were brought to an end by the Bølling-Allerød Interstadial during which ice retreated into the high Alps [*Ohlendorf*, 1998]. Glaciers readvanced at the end of the Bølling-Allerød. The Egesen Stadial, time correlative with the Younger Dryas (YD), is characterized by valley and cirque glaciers [*Ivy-Ochs et al.*, 1996; *Kerschner et al.*, 2000]. Climate then warmed again following the YD. While glaciers did advance numerous times in the Holocene during Kartell, Kromer, and Little Ice Age Stadials [*Sailer*, 2001; *Kerschner et al.*, 2006], they never again reached their YD extents. Several Holocene glacier advances have been dated, however, that indicate that glaciers were larger than today in these phases [*Hormes et al.*, 2001].

2.2. Recent Geodetic Uplift Pattern

[10] The recent vertical movements of the Central Alps of Switzerland relative to the benchmark at Aarburg have been recorded since 1905 and are displayed in Figure 2 [*Schlatter et al.*, 2005]. In the following, we will term these vertical movements "rock uplift rates," because they are measured with respect to an arbitrary benchmark, which is defined as being stable in altitude relative to the area of interest.

[11] In some regions of the Alps, especially in the Central Alps, rock uplift rates exceed 1.0 mm/a, and decrease to 0.2 mm/a in the foreland of the Central Alps [*Schlatter et al.*, 2005]. In this paper, we have used the data set from *Schlatter et al.* [2005] throughout. It is generally assumed that the pattern of uplift is the result of deep crustal processes, since the contour lines of the uplift are parallel to the Alpine strike [*Schlunegger and Hinderer*, 2001], and because the tip of the Adriatic indenter is located beneath the area of maximum uplift [*Schmid and Kissling*, 2000]. However, the mechanism that controls the rate of rock uplift is subject of an intense debate. *Gudmundsson* [1994] suggested that a transient isostatic rebound reaction of the crust from the removal of the Pleistocene ice sheet could have caused a significant part of the present uplift of the Central Alps [*Gudmundsson*, 1994]. This view was challenged by *Persaud and Pfiffner* [2004], who argued that the length scale of the recent uplift pattern exceeds that expected from postglacial rebound when using a standard mantle viscosity. They also noted that the recent pattern of uplift resembles that of apatite fission track age distribution, which would suggest long-term stability of the uplift process at the Ma timescale. These authors suggested a rapid postmelting uplift pulse of ~200 m and proposed that the present uplift is indeed caused by deep crustal processes [*Persaud and Pfiffner*, 2004]. Recently, *Barletta et al.* [2006] suggested that ~0.5 mm/a of a total uplift rate of 0.8 mm/a is caused by recent glacier shrinkage while *Champagnac et al.* [2007] attributed a significant fraction (~50%) of the present-day vertical movement to the isostatic response to enhanced erosion during Plio-Quaternary times.

2.3. Sample Characteristics

2.3.1. Prerequisites

2.3.1.1. LGM Moraine Deposits

[12] We tested the potential bias on catchment-wide denudation rates introduced by the admixing of LGM and Younger Dryas moraine deposits into streams by measuring the concentration of subsurface moraine material (see Figure 1 and Table 2). We sampled one LGM moraine from the Swiss Mittelland (samples Saf 1-1 and 1-2), one YD moraine in the Central Alps (sample Herens), one moraine from Findelen Glacier in the Southern Valais Alps (sample Fin 4), and one glaciofluvial valley infill of max. LGM age in the Central Alps (sample Mela 1 GF).

[13] The samples Saf 1-1 and Saf 1-2 are replicate samples from the Aare LGM moraine, Swiss Mittelland, taken in a gravel pit at 20 m depth. The moraine was deposited 18000 ± 3000 a ago during the Late Würmian glaciation (C. Schluechter, personal communication, 2005). The sample Herens was taken from a lateral compression till of YD age inside a gravel pit near the river Borgne (Val d' Herens, Southern Valais Alps) at a depth of 3 m. Sample Fin 4 was taken from inside a lateral moraine of Findelen Glacier, Monte Rosa/Dufourspitze, Southern Valais Alps, 5 m below the tip of the moraine. The deposition age is 2000 ± 600 a [*Roethlisberger and Schneebeli*, 1979]. Sample Mela 1 GF was taken from the bottom of a ~45 m thick glaciofluvial valley infill of LGM or younger age (<18000 a) of the Melezza at Dissimo (Centovalli, Central Alps).

2.3.1.2. Recent Glacial Erosion Products

[14] To assess the nuclide concentrations of recent glacial erosion products, we sampled sediment produced by recent or young glaciers. Sample Fin 2 is sediment directly from the Findelen Glacier outlet snout. The samples Miné 4-1

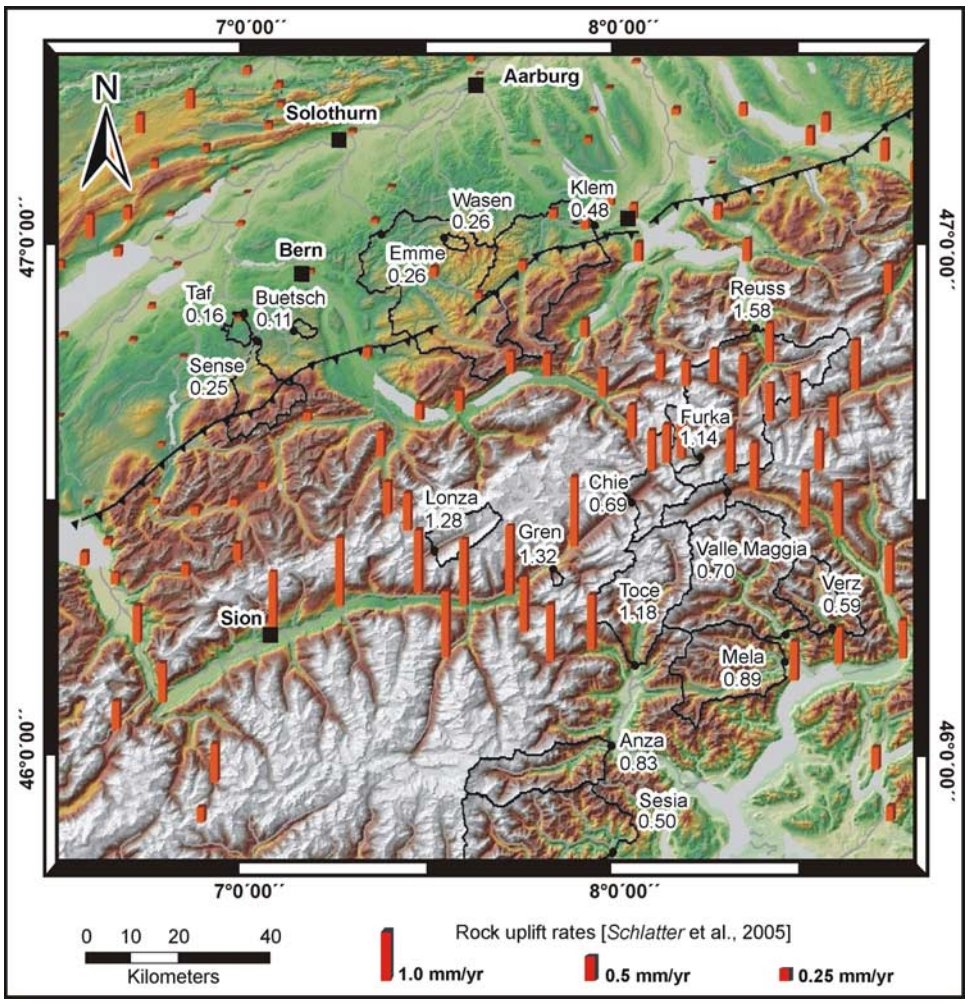

Figure 2. Recent vertical movements in the Central Alps of Switzerland. Bar heights give rate of rock uplift (based on *Kahle et al.* [1997] and revised by *Schlatter et al.* [2005] measured relative to the benchmark at Aarburg. Also shown are locations of catchments sampled for catchment-wide cosmogenic nuclide analysis with abbreviated sample names (see Table 1, except Maggia tributaries, moraine samples, and glacial sediment samples). Denudation rates are given in mm/a; for catchments where two or more denudation rates were measured, the mean value is given.

and 4-2 are separate samples of glacial outwash sediment collected at the southern glacier snout of Mont Miné Glacier. Sample Miné 5 also consists of glacially outwashed sediment and was taken from the northern outlet of the glacier. Sample Miné 6 is a sample from a young lateral moraine of Mont Miné Glacier at the eastern side of the valley, its depositional age being approximately ~300 a (Little Ice Age). Sample Fin 1 consists of well-rounded quartzite pebbles that were presumably eroded from a quartzite occurrence from the topmost ridge above Findelen Glacier.

[15] Furthermore, we sampled the two heavily glaciated catchments, Massa and Matt, of rivers that directly drain the Great Aletsch Glacier (river Massa, 66% glaciated area) and the Gorner/Findelen Glaciers (river Mattervispa, 54% glaciated area) in the Southern Valais Alps.

2.3.1.3. Appropriate Catchment Sizes for Cosmogenic Sampling

[16] In the presently nonglaciated Maggia valley we tested whether trunk stream sampling of a U-shaped valley is a feasible strategy, whether cosmogenic denudation rate estimates are in the same order of magnitude as erosion rates from lake fills and river loads (Table 3), and whether tributaries of various sizes yield internally consistent denudation rates. We attempted to assign an optimal catchment size for representative denudation rate measurements. We therefore sampled the Maggia trunk stream at three different locations in the valley and eight different tributaries within Valle Maggia. The Maggia catchment is composed of almost one single granitoid gneissic lithology, with minor sequences of ultrabasic rocks and eclogites enclosed, so that lithologic effects on denudation rate estimates are minimized.

2.3.2. Characteristics of Basins Sampled Along an Alpine North-South Traverse

2.3.2.1. High-Alpine Basins

[17] We sampled several trunk streams in the high Alps of Switzerland and Northern Italy, e.g., the Reuss and the Rhône rivers. Samples were taken during low flow from the active channel. The spatial extent of modern glaciers in our

Table 2. Cosmogenic Nuclide Analytical and Derived Denudation Rate Data

Sample Type	Sample Name	Sample Weight, g	^{10}Be Concentration,[a] $\times 10^4$ at/g$_{(Quartz)}$	^{10}Be Concentration,[b] SLHL Normal, $\times 10^4$ at/g$_{(Quartz)}$	Total Nuclide Production Rate,[c] at/g a	Skyline Shielding Factor	Snow/Ice Shielding Factor[d]	Denudation Rate,[e] mm/a	Apparent Age,[f] a
LGM or younger moraine samples	Saf 1-1	76.1	2.64 ± 0.70	1.42 ± 0.43	10.1	0.99	1.00	0.32 ± 0.09	2560
	Saf 1-2	59.0	2.29 ± 0.26	1.22 ± 0.21	10.1	0.99	1.00	0.37 ± 0.05	2220
	Herens	23.4	0.79 ± 0.27	0.06 ± 0.12	36.8	0.97	1.00		110
	Fin 4	61.1	2.30 ± 0.41	0.20 ± 0.04	63.0	0.99	1.00	1.87 ± 0.33	360
	Mela 1 GF	52.2	0.13 ± 0.17	0.04 ± 0.06	17.4	0.99	0.97		80
Recent glacial sediment samples	Fin 1	18.4	7.78 ± 2.43	0.72 ± 0.23	59.6	0.96	0.97	0.52 ± 0.16	1320
	Fin 2	27.7	2.32 ± 0.98	0.22 ± 0.09	59.3	0.97	0.99	1.73 ± 0.74	390
	Miné 4-1	45.1	0.52 ± 0.26	0.06 ± 0.03	48.7	0.99	0.87	6.44 ± 3.18	110
	Miné 4-2	75.1	1.15 ± 0.37	0.13 ± 0.04	48.7	0.99	0.87	2.89 ± 0.90	240
	Miné 5	77.3	1.25 ± 0.50	0.14 ± 0.06	48.7	0.99	0.87	2.68 ± 1.06	260
	Miné 6	40.3	1.90 ± 1.06	0.22 ± 0.12	48.7	0.99	0.87	1.76 ± 0.98	390
	Massa	55.1	0.76 ± 0.39	0.08 ± 0.04	52.0	0.99	0.41	4.65 ± 2.34	150
	Matt	57.9	3.01 ± 1.22	0.33 ± 0.13	49.9	0.97	0.50	1.13 ± 0.46	610
Maggia sediment samples	Mag 1	45.7	3.05 ± 0.62	0.94 ± 0.19	17.9	0.95	0.99	0.41 ± 0.09	1820
	Mag 2	45.7	3.55 ± 0.59	1.04 ± 0.17	19.0	0.93	0.98	0.36 ± 0.06	2070
	Mag 4	49.3	1.53 ± 0.38	0.33 ± 0.08	25.9	0.97	0.94	1.12 ± 0.28	650
	Mag 8	46.6	2.10 ± 0.41	0.40 ± 0.08	28.7	0.92	0.85	0.78 ± 0.15	940
	Mag 10	47.5	2.38 ± 0.41	0.44 ± 0.08	29.9	0.92	0.92	0.77 ± 0.13	940
	Mag 11-2	41.4	2.10 ± 0.36	0.47 ± 0.08	26.1	0.93	0.91	0.77 ± 0.13	950
	Mag 11-4	52.4	1.93 ± 0.31	0.44 ± 0.07	24.6	0.93	0.92	0.80 ± 0.13	920
	Mag 13	48.0	3.24 ± 0.54	0.44 ± 0.07	41.0	0.97	0.79	0.69 ± 0.12	1030
	Mag 16	47.4	1.68 ± 0.43	0.33 ± 0.08	28.5	0.94	0.91	1.06 ± 0.27	690
	Mag 17	45.6	5.06 ± 0.73	0.98 ± 0.14	28.6	0.93	0.91	0.35 ± 0.05	2090
	Mag 18	46.1	3.27 ± 0.45	0.57 ± 0.08	31.8	0.94	0.91	0.60 ± 0.08	1190
North-south traverse samples	Anza	43.9	1.88 ± 0.58	0.41 ± 0.13	25.4	0.93	0.88	0.83 ± 0.26	890
	Sesia	37.8	2.90 ± 0.56	0.75 ± 0.14	21.3	0.94	0.97	0.50 ± 0.09	1490
	Toce a	89.2	1.95 ± 0.33	0.38 ± 0.06	28.4	0.94	0.89	0.89 ± 0.15	820
	Toce b	62.5	1.19 ± 0.27	0.23 ± 0.05	28.4	0.94	0.89	1.46 ± 0.33	500
	Verz a	46.4	2.44 ± 0.45	0.59 ± 0.11	22.9	0.92	0.94	0.60 ± 0.11	1230
	Verz b	38.2	2.47 ± 0.51	0.59 ± 0.12	22.9	0.92	0.94	0.59 ± 0.12	1250
	Mela 1	60.1	0.96 ± 0.19	0.31 ± 0.06	17.3	0.97	0.97	1.28 ± 0.26	590
	Mela 2	32.2	1.07 ± 0.40	0.37 ± 0.14	15.9	0.96	0.95	1.05 ± 0.39	740
	Mela 3a	44.3	1.84 ± 0.44	0.58 ± 0.14	17.5	0.95	0.97	0.66 ± 0.16	1140
	Mela 3b	45.9	2.19 ± 0.42	0.69 ± 0.13	17.5	0.95	0.97	0.56 ± 0.10	1400
	Lonza	63.3	1.42 ± 0.35	0.20 ± 0.05	40.0	0.94	0.65	1.28 ± 0.32	580
	Gren	36.7	1.30 ± 0.42	0.26 ± 0.08	27.7	0.95	0.90	1.32 ± 0.43	550
	Chie	51.2	2.56 ± 0.62	0.37 ± 0.09	37.8	0.96	0.65	0.69 ± 0.17	1080
	Furka	61.3	1.68 ± 0.29	0.22 ± 0.04	41.3	0.97	0.65	1.14 ± 0.20	640
	Tic a	48.4	1.95 ± 0.45	0.33 ± 0.08	32.7	0.96	0.83	0.97 ± 0.23	740
	Tic b	50.4	2.98 ± 0.57	0.50 ± 0.10	32.7	0.96	0.83	0.63 ± 0.12	1140
	Reuss a	47.9	1.45 ± 0.43	0.25 ± 0.07	32.5	0.94	0.84	1.29 ± 0.38	560
	Reuss b	40.8	1.00 ± 0.42	0.17 ± 0.07	32.5	0.94	0.84	1.87 ± 0.79	390
	Klem a	47.0	2.43 ± 0.48	1.02 ± 0.20	13.1	0.99	0.98	0.42 ± 0.08	1900
	Klem b	39.6	1.88 ± 0.46	0.79 ± 0.19	13.1	0.99	0.98	0.54 ± 0.13	1470
	Buetsch 1	57.0	7.00 ± 1.14	3.96 ± 0.64	9.8	1.00	0.99	0.11 ± 0.02	7260
	Buetsch 2	52.4	8.06 ± 0.89	4.57 ± 0.50	9.8	1.00	0.99	0.10 ± 0.01	8370
	Emme	59.0	3.54 ± 0.42	1.71 ± 0.20	11.5	0.99	0.99	0.26 ± 0.03	3160
	Wasen 1-1	54.3	3.13 ± 0.75	1.44 ± 0.35	12.0	0.99	0.99	0.30 ± 0.07	2660
	Wasen 1-2	26.2	3.38 ± 0.59	1.56 ± 0.27	12.0	0.99	0.99	0.28 ± 0.05	2870
	Taf	74.9	4.32 ± 0.50	2.96 ± 0.34	8.1	1.00	0.99	0.16 ± 0.02	5400
	Sense	24.5	3.99 ± 0.75	1.52 ± 0.28	14.5	0.98	0.96	0.25 ± 0.05	3110

[a]Corrected for blank, with combined analytical and blank error. For buried samples, nuclide concentrations corrected for postdepositional irradiation are given in Table S1.
[b]Calculated for blank, with uncorrected mean catchment production rate (see next column) and a SLHL production rate of 5.53 atoms/g quartz.
[c]Uncorrected production rates.
[d]Not applied to old moraine and recent glacial sediment samples.
[e]For intermethod comparison, combined errors for AMS measurements, blank subtraction, and a constant error for scaling factor (5%).
[f]Corresponds to the time spent in the uppermost ~60 cm of an eroding rock layer.

Table 3. Denudation Rate Data From Lake Infills, River Loads, and Delta Growth

				Since LGM	Modern	
				Lake Fills	River Load	Delta Growth
River	Location of Gauging Station	Lake	Drainage Area of River,[a] km^2	Mechanical Denudation Rate,[a] mm/a	Total Denudation Rate,[b] mm/a	Total Denudation Rate,[a,b] mm/a
Aare	Brienzwiler	Brienzersee	554	0.38	0.11	0.19
Kander	Hondrich	Thunersee	1120	-	0.36	-
Linth	-	Zürichsee		0.73	-	-
Linth	Mollis	Walensee	530	-	0.09	0.16
Lütschine	Gsteig	Brienersee	380	0.82	0.20	0.06
Melchaa	-	Sarnersee	72	0.37	-	-
Reuss	Seedorf	Urnersee	832	0.56	0.03	-
Seez	-	Walensee	269	0.96	-	-
Rhone	Porte du Scex	Lac Léman	5520	0.95	0.15	-
Adda	Tirano	Lago di Como	906	0.85	0.10	-
Cassarate	-	Lago di Lugano	73	-	-	0.16
Maggia	Locarno	Lago Maggiore	926	0.51	0.22	0.18
Ticino and Verzasca	Bellinzona	Lago Maggiore	1515	0.79	0.13	0.11
Dora Baltea River[c]	Dora Baltea[c]	-	3264[c]	-	0.12[c]	-

[a]From *Hinderer* [2001].
[b]Recalculated from *Hinderer* [2001] using a density of 2.5 g/cm^3.
[c]From *Vezolli* [2004].

catchments varies strongly (Table S1)[1], from presently nonglaciated catchments (e.g., the catchment of the Verzasca) to ~30% of glaciation in the catchment of the Lonza (draining the Aletsch Glacier). The bulk lithology of these catchments is relatively uniform; all studied basins within the high Alps display metamorphosed crystalline lithologies (see Figure 1). The catchment of the Reuss also comprises Molasse sediments (conglomerates and sandstones) of lower erosional resistance [*Schlunegger and Hinderer*, 2001]. The Aar and Gotthard Massifs (samples Furka, Chie, and Lonza) contain plutonic rocks such as granites, quartzdiorites, and granodiorites. South of the Aar and Gotthard Massifs, metasedimentary sequences comprising schists and ophiolites crop out along a thin ~10 km stretch (sample Gren).

2.3.2.2. Swiss Mittelland Basins

[18] The lithology of the Mittelland catchments consists of Molasse sediment, which contains heterogeneous sedimentary sequences of sandstones, shales, and carbonate conglomerates with low erosional resistance [*Schlunegger and Hinderer*, 2001]. We particularly targeted areas that were formerly glaciated and others that were not ice covered during the LGM. The small (<25 km^2) Mittelland catchments of the Tafersbach, the Liechtguetbach (samples Taf and Wasen 1-1 and 1-2, respectively), as well as the bigger (>160 km^2) catchments of the Kleine Emme, the Emme, and the Sense (samples Klem, Emme, and Sense, respectively) have been glaciated during the LGM, whereas the catchment of the Bütschelbach (samples Buetsch 1 and 2) stayed ice free throughout [*Jäckli*, 1970]. This set of data gives a good selection of possible topographic and climatic basin features and allows comparison of the derived denudation rates with paleodenudation estimates from apatite fission track and recent rock uplift rates. A more detailed analysis of the denudation rates and post-LGM geomorphic evolution of the Mittelland Molasse area is provided by *Norton et al.* [2007].

[1]Auxiliary materials are available in the HTML. doi:10.1029/2006JF000729.

2.4. Lab Processing and Uncertainty Assessment

[19] The bulk samples were sieved into narrow grain size ranges (see Table 1) and ~50 g of quartz were separated from the bulk sediment using chemical (selective decomposition with weak HF) and magnetic separation techniques. The separation of ^{10}Be was achieved by using an element separation method described by *von Blanckenburg et al.* [1996] and simplified by *von Blanckenburg et al.* [2004]. $^{10}Be/^{9}Be$ ratios were measured with accelerator mass spectrometry at PSI/ETH Zurich and corrected as described by *Synal et al.* [1997]. Ca. 300 μg of ^{9}Be from a MERCK© $BeSO_4$ carrier were added to each sample. This carrier was determined to contain a $^{10}Be/^{9}Be$ ratio of $1.10 \pm 0.66 \times 10^{-14}$. Samples Mag 11-2, Mag 11-4, Mela 1, Mela 1 GF and Mela 2 were treated with a carrier derived from a phenakite mineral, giving a measured $^{10}Be/^{9}Be$ ratio of $0.55 \pm 0.28 \times 10^{-14}$. The blanks were subtracted and their errors propagated into all concentrations. The calculated ^{10}Be concentrations with combined analytical and blank errors are given in Table 2. Denudation rate uncertainty estimates include a 5% error on scaling law for intermethod comparison. An additional potential uncertainty of 30% on denudation rates is introduced by grain size effects, shielding effects due to temporally and spatially nonuniform snow distribution, nonsteady state effects after glaciation and for catchments with >10% glaciation (samples Lonza, Chie, Furka, and Reuss). This uncertainty cannot be quantified accurately and is therefore not included in Table 2.

3. Methodological Principles

3.1. Spatially Averaged Denudation, Calculation of Production Rates, and Corrections Applied

3.1.1. Spatially Averaged Denudation Rates From Cosmogenic Nuclides in River Sediment

[20] Cosmogenic ^{10}Be is mainly produced from ^{16}O within mineral grains by bombardment by secondary cosmic rays [*Lal and Peters*, 1967]. The ^{10}Be nuclide concen-

tration of minerals is inversely proportional to the denudation rate of the surface [*Lal*, 1991]:

$$C = \frac{P_0}{\lambda + \frac{\rho\varepsilon}{\Lambda}}\left(1 - \exp^{-\left(\lambda + \frac{\rho\varepsilon}{\Lambda}\right)t}\right) \quad (1)$$

where C is the concentration of in situ–produced cosmogenic ^{10}Be (at/g$_{(Quartz)}$), P_0 is the production rate at the Earth's surface scaled for latitude and altitude (at/g$_{(Quartz)}$a), λ is the ^{10}Be decay constant (1/a), ρ is the rock density (g/cm^3), ε is the denudation rate (cm/a), Λ is the mean cosmic ray attenuation length (157 g/cm^2), and t is the time (a) since the initial exposure to cosmic rays. In the Alps, this would correspond to the melting of LGM glaciers, for example. About 63% of the cosmogenic nuclides are produced within the cosmic ray attenuation length, equal to 60 cm of a rock with a density of 2.7 g/cm^3 [*Lal*, 1991]. The continuous removal of a rock layer equal to several attenuation lengths by constant denudation leads to a steady state ^{10}Be nuclide concentration in the catchment. In this case, the rate of nuclide production equals the rate of nuclides exported by sediment and the ^{10}Be concentration may be simply expressed as [*Lal*, 1991]

$$C = \frac{P_0}{\lambda + \frac{\rho\varepsilon}{\Lambda}} \quad (2)$$

[21] At cosmogenic steady state, cosmogenic ^{10}Be in riverborne quartz records a time-integrated spatially averaged denudation rate, which represents the fluvially mixed erosion products of all processes within a drainage basin [*Bierman and Steig*, 1996; *Granger et al.*, 1996]. The denudation rate integrates over the time it takes to remove one attenuation length (e.g., 60 cm of bedrock). This integration timescale is called the ''apparent age'' and it depends on the denudation rate itself. In the high Alps, typical denudation rates are 1.5–0.5 mm/a, which correspond to a timescale of ~400–1200 a.

[22] Since cosmogenic nuclides measure the denudation rate of bedrock including both mechanical erosion and chemical weathering, we use the term ''denudation'' throughout this paper. A tectonic denudation component, however, is not included. Recent reviews of the method can be found in work by *Bierman and Nichols* [2004] and *von Blanckenburg* [2005].

3.1.2. Production Rates

[23] The cosmogenic nuclide production rates and adsorption laws were those of *Schaller et al.* [2002], while scaling for altitude and latitude of our sampling sites was done following *Dunai* [2000]. We did not specifically correct for variations in Earth's magnetic field or an enrichment of quartz during weathering. The influence of a varying geomagnetic field intensity is negligible at latitudes of the Central Alps [*Masarik et al.*, 2001], and we assumed that quartz enrichment [*Riebe et al.*, 2001] is negligible because of the short weathering intervals.

[24] For our LGM subsurface moraine samples, postdepositional irradiation had to be corrected for, because muons penetrate deep into the subsurface [*Brown et al.*, 1995a]. The depth dependence of nuclide production by postdepositional irradiation has been calculated using a formalism of *Schaller et al.* [2002]:

$$C_{dep} = \left[\left(P_{Nuc}(0) * \sum_{i=1}^{2} a_i * \exp^{\frac{-z*\rho}{b_i}}\right) + \left(P_{\mu stopped}(0) * \sum_{j=1}^{3} a_j * \exp^{\frac{-z*\rho}{b_j}}\right) + \left(P_{\mu fast}(0) * \sum_{k=1}^{3} a_k * \exp^{\frac{-z*\rho}{b_k}}\right)\right] * \left(\frac{1 - e^{-\lambda * t_{dep}}}{\lambda}\right) \quad (3)$$

where $P_{Nuc}(0)$, $P\mu_{stopped}(0)$ and $P\mu_{fast}(0)$ (at/g$_{(Quartz)}$a) are the production rates of cosmogenic nuclides by spallation, stopped and fast muons, respectively. Z (cm) is the depth below surface, t_{dep} (a) is the time since the deposition of the material, $a_{i,j,k}$ (dimensionless) and $b_{i,j,k}$ (g/cm^2) are coefficients used for the depth scaling of the production rates (coefficient values given by *Schaller et al.* [2002]).

3.1.3. Corrections for Skyline Shielding and Shielding Due to Snow and Ice

[25] Corrections of the production rates for topographic shielding were necessary because landscapes like the Central Alps feature considerable relief. An object on the surface of a flat, level landform has an unobstructed view of the sky in all directions and therefore will receive maximum incoming radiation [*Dunne et al.*, 1999]. Since this is not the case in landscapes with highly sloped surfaces, the decreased incoming flux of radiation resulting in reduced production rates has to be considered [*Dunne et al.*, 1999]. For this study, we employed an algorithm that calculates the reduction of the intensity of incoming radiation for a DEM pixel inside a catchment using the hypsometry (e.g., the elevation versus area distribution) of each catchment as derived from the SRTM DEM with a grid resolution of 90 m [after *Heidbreder et al.*, 1971]:

$$S = 1 - \frac{1}{360^\circ}\sum_{i=1}^{n} \Delta\phi_i \sin^{m+1}\theta_i \quad (4)$$

where S is the shielding factor for a set of n obstructions, each with a corresponding inclination angle θ_i with an extent through an azimuth of the incoming radiation $\Delta\phi_i$, m is an experimentally determined constant for which we used a value of 2.3 [*Dunne et al.*, 1999]. The shielding algorithm employs 360° shielding for each pixel on the basis of 5° steps for the azimuth angle. The resulting catchment mean skyline correction factor varied between 1 for ridges or valleys of low relief (e.g., no correction) and 0.92 for valleys in steep catchments, which would in this case result in a production rate reduction of 8% (see Table 2).

[26] Corrections of the production rates for shielding due to snow and ice were necessary because glaciation and significant snow cover reduce cosmogenic nuclide production rates in bedrock [*Schildgen et al.*, 2005]. We calculated a combined snow and ice correction factor for each pixel. Snow correction factors are based on mean averages of monthly resolved snow thicknesses for the years 1983–2002 [*Auer*, 2003]. For ice correction calculation, we used the present-day glacial extent to calculate a mean correction factor. This was based on the assumption that during the

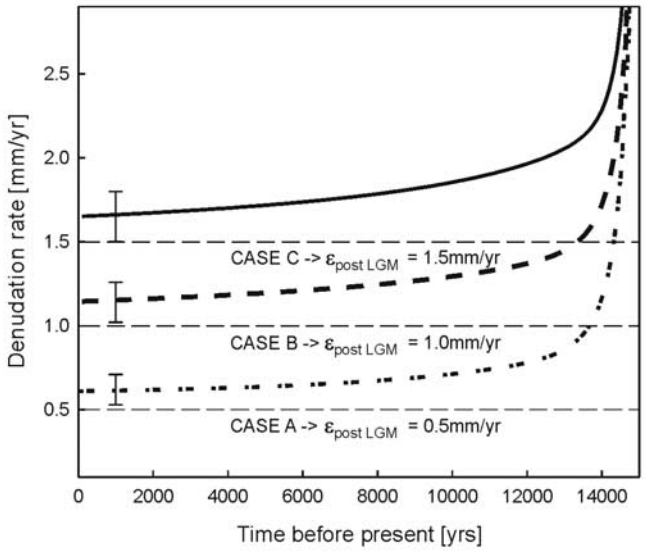

Figure 3. Numerical modeling of the approach of cosmogenic nuclides to steady state after zeroing by glaciation at t = 15 ka BP on the basis of three different denudation histories (0.5, 1.0, and 1.5 mm/a); also given are typical analytical error bars. The analysis shows that cosmogenic steady state is attained within limits of error for the 1.5 mm/a and the 1.0 mm/a case after 15 ka.

considered time span, glacial advance and recession might have been counterbalancing each other [*Hormes et al.*, 2001]. As will be shown below, we suggest that denudation rates are robust if the area glaciated is <10% of a catchment. Therefore the possible bias introduced by this assumption would add only a minor error. Calculations were carried out using a formalism similar to *Lal* [1991]:

$$K = \exp^{\frac{-\rho * z}{\Lambda}} \quad (5)$$

where K is the correction factor for snow independent of the prevailing total production rate, ρ is the maximum density of 0.3 g/cm^3 for old, compacted snow [*Roebber et al.*, 2003; *Ware et al.*, 2006], z is the snow thickness (cm), which varied for each pixel on the basis of digitized snow depths with a spatial resolution of 1 km from *Auer* [2003], Λ is the mean cosmic ray attenuation length (157 g/cm^2). The correction was done by multiplying the nucleonic surface production rate by this factor, while leaving all other coefficients of *Schaller et al.* [2002] constant. This means that we ignored the correction for the reduced muonic production, because the attenuation of both fast and stopped muons in snow is negligible. The influence of snow cover on production rates with respect to neutron-backscattering effects at the snow-rock interface [*Schildgen et al.*, 2005] has also not been taken into account with this approach. However, we suggest that the overall effect on the calculation of denudation rates is negligible. The nucleonic nuclide production rate was set to zero for pixels covered by ice. The area of recent glaciation in Switzerland was digitized from topographic maps and calculated from public domain GIS data (source: ESRI).

[27] In order to evaluate the effect of today's glaciation on cosmogenic nuclide-derived denudation rates, we have measured the ^{10}Be concentration of present-day glacial outwash (see Section 2.3). We did not correct the total production rate for these catchments (see Table 2) in order to account for the effect of glaciation as a potential perturbation on this material. In Table 2, we give the total, uncorrected production rate for each catchment as well as the calculated mean correction factors on the production rate for snow/ice and skyline shielding. Cosmogenic nuclide-derived denudation rates for Maggia sediment samples and traverse samples were calculated on the basis of these correction factors. The total correction for sediment samples amounts to 1% for Mittelland samples, 5–10% for southern Central Alps samples, and up to 35% for partially glaciated samples in the highest Central Alps. Given that the latter correction factors are based on the modern glacial extent, denudation rates might be overestimated if the glaciers had a larger extent within the sampling timescale. For all non-glaciated catchments, the error introduced is small.

3.2. Assessment of Potential Perturbations on Denudation Rate Estimates in Complex Glaciated Mountain Ranges

3.2.1. Approach to Cosmogenic Steady State After Surface Zeroing by Glaciation

[28] Cosmogenic nuclide-derived denudation rates in the high Alps are potentially biased by former (e.g., LGM) and recent glaciation that result in a cosmogenic nonsteady state situation. Therefore an assessment of whether the production and the export of nuclides have reached steady state after a possible complete zeroing of surface concentrations by glacial abrasion and ice shielding is necessary. We have performed numerical modeling of the approach of cosmogenic nuclide inventories to steady state rates following glaciation by assuming zero initial nuclide concentration within the entire rock column. Calculations were carried out by integrating the ^{10}Be nuclide production during small time steps over the attenuation path length while material moves toward the surface by denudation. We simulated three different denudation exposure histories and subsequent denudation at 15 ka BP of 0.5, 1.0, and 1.5 mm/a from t = 15 ka BP until today using the production and adsorption terms from *Schaller et al.* [2002], which are based on nucleonic and muonic production, and equation (2). Figure 3 shows that the cosmogenic nuclide-derived denudation rates approach steady state depending on the prescribed denudation rate, and, although never quite reaching it, are within the typical analytical error of our measured denudation rates. Other workers [*Parker and Perg*, 2005] have carried out a similar model and have found that with comparable model parameters, it takes even less time for a landscape to arrive at nuclide steady state after major perturbations. In our opinion, this can be attributed to the fact that *Parker and Perg* [2005] did not account for muonic production in their model. Production of nuclides from muons leads to much longer timescales with respect to steady state achievement because of their deep penetration depth.

3.2.2. Cosmogenic Nuclide Inventory of Incorporated Moraine Material and Recent Glacial Erosion Products

[29] We acknowledge that recently glaciated catchments suffer from nonsteady state behavior due to glacial erosion. Therefore we tested the potential bias introduced by the admixing of denudation products into streams by measuring

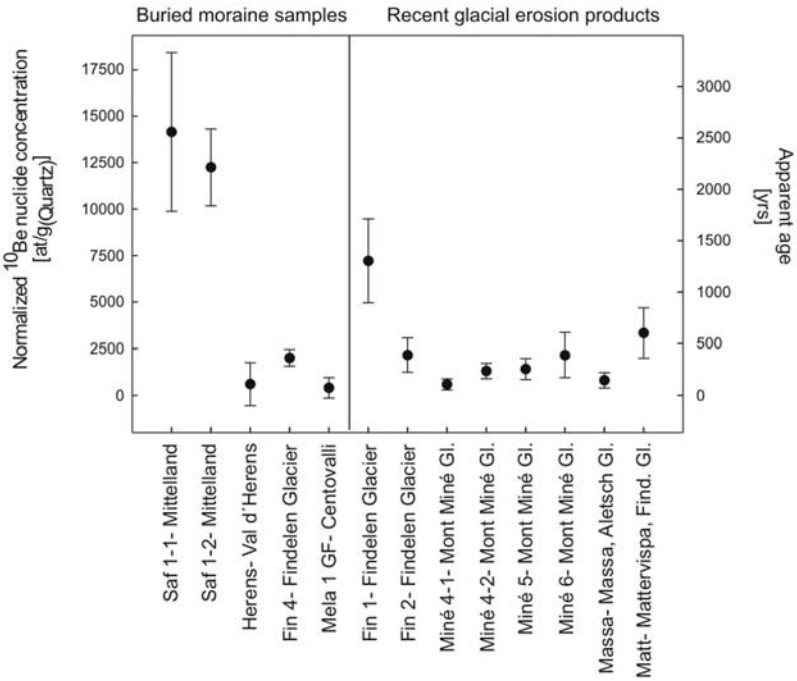

Figure 4. Nuclide concentrations of buried moraines and glacial sediments scaled to SLHL (left axis); right axis gives corresponding "apparent age" that would result if sediment were exposed at the surface. For glacial sediment nuclide concentrations, the percentage of glaciated area of each catchment is decreasing from left to right, e.g., from 75% to 55%.

the concentration of both LGM and recent subsurface moraine material, as well as modern products of glacial erosion, e.g., sediment outwashed from glacier snouts. The results are given in Table 2 and Figure 4. In order to allow for comparison of results from various altitudes, we scaled the nuclide concentrations to sea level high latitude (SLHL; see Figure 4), using a production rate at sea level of 5.53 at/$g_{(Quartz)}$a [*Schaller et al.*, 2002]. Measured and normalized nuclide concentrations are also given in Table 2. The measured moraines of LGM and younger age reveal a broad range of cosmogenic nuclide concentrations.

[30] Replicate samples Saf 1-1 and 1-2 (Swiss Mittelland Aare LGM moraine material) give normalized nuclide concentrations at SLHL corrected for postdepositional irradiation that are identical within one sigma error (for nuclide concentrations see Table 2). We speculate that the glacial advance led in part to the incorporation of overridden regolith, which comprised periglacial soils in the Molasse basin that would have been irradiated prior to the ice advance. This would explain the comparatively high nuclide concentration that would correspond to an apparent paleodenudation rate of ~0.3 mm/a; or an apparent exposure age of ~2200 a. As shown in section 4.1, this is similar to today's Mittelland denudation rate. The sample Herens consists of subglacial consolidated clay till, which is assumed to have formed during YD because of denudation of shielded and already heavily abraded or plucked bedrock, so that the inherited nuclide concentration is zero within limits of error. For sample Fin 4 (Findelen glacier, lateral moraine, 2000 ± 600 a old), it is assumed that the nuclide concentration we measured is a mixture from several sources, e.g., material from the exposed side valleys of the glacier (with relatively high nuclide concentrations) mixed with that from beneath the glacier (with relatively low concentrations), resulting in a mean nuclide concentration which might as well be representative for sediment mixing processes at glaciers like the Findelen. The apparent age would be ~350 a. The inherited nuclide concentration of sample Mela 1 GF (LGM or younger glaciofluvial sediment in the upper Centovalli, southern Central Alps) is zero within limits of error. The deposit is assumed to have formed from glacial abrasion of shielded and already heavily abraded bedrock.

[31] Sampling of recent glacial erosion products of the Findelen Glacier (sample Fin 1; well-rounded quartzite pebbles from topmost ridge of glacier) gives a comparatively high nuclide concentration comparable with an apparent denudation rate of ~0.5 mm/a or an apparent exposure age of 1300 a (for nuclide concentrations, see Table 2 and Figure 4). This is probably caused by the admixture of material from exposed and slowly eroding ridges surrounding the glacier. Sample Fin 2 (outwash from glacier snout) also gives a rather high nuclide concentration corresponding to a denudation rate of 1.7 mm/a or an apparent age of 390 a; the concentration is too high for shielded material and suggests the incorporation of exposed denudation products. Samples Miné 4-1 and 4-2 (separate samples from southern snout) are two samples from exactly the same location but reveal nuclide concentrations that vary within a factor of two (apparent ages of 110 and 240 a, respectively), evidently confirming the heterogeneous nature of glacial erosion processes. Sample Miné 5 (northern snout, 260 a) gives similar nuclide concentration as Miné 4-1 and 4-2. Sample Miné 6 (lateral moraine of Mont Miné Glacier, its depositional age being ~300 a) gives a

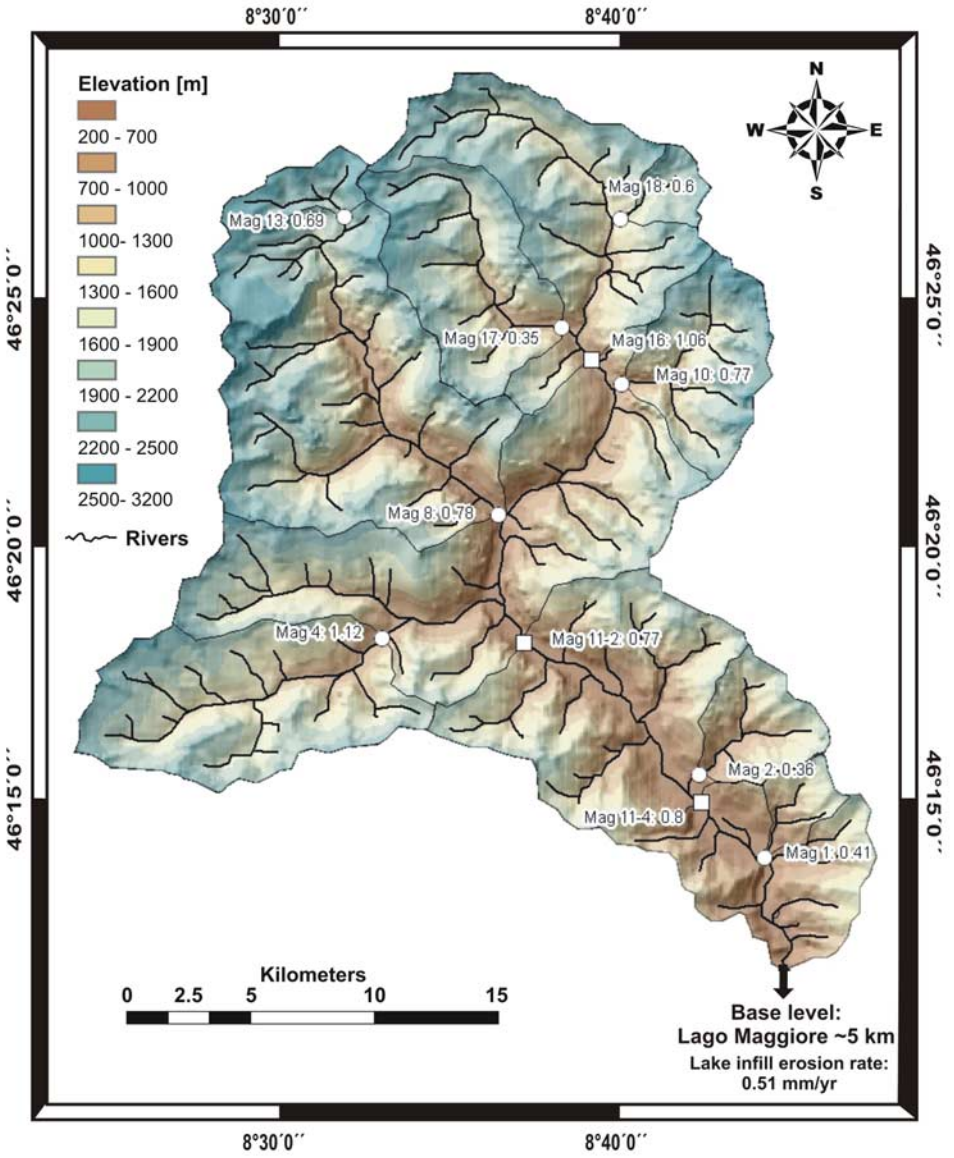

Figure 5. Catchment of the Maggia derived from a 90 m SRTM grid. Shown are sampling locations and corresponding cosmogenic nuclide-derived denudation rates in mm/a. Squares indicate trunk stream samples, and circles indicate tributary samples. A mechanical denudation rate calculated from the infill of Lago Maggiore is 0.51 mm/a since the LGM [*Hinderer*, 2001].

somewhat higher nuclide concentration (corresponding to an apparent age of 390 a) than other Miné samples. It can only be assumed that during glacial advance during the Little Ice Age, exposed bedrock was abraded and deposited as a moraine. Nuclide concentrations of all Miné Glacier samples are very low and apparent ages would be around 200 a.

[32] The measured nuclide concentrations and apparent ages of samples Massa (150 a) and Matt (610 a; River Massa draining the Great Aletsch Glacier and river Mattervispa draining the Gorner/Findelen Glaciers, respectively) are within the same range as those of sediment directly from glacial outlets. This suggests that in all cases sediment from highly glaciated catchments contains previously exposed material that is currently being remobilized and eroded.

[33] These results allow for the following first-order implications. Glacial sediment is subject to a range of exposure histories and no a priori concentration can be predicted. It has been demonstrated for the Mittelland that high-concentration samples of LGM age are compatible with the denudation rates of the respective surrounding nonglaciated areas. This hints at a large fraction of nonglacial erosion products in glacial outflows of Alpine warm-based glaciers. Therefore neither the assumption of zero concentration beneath the area covered by recent glaciers (because glaciers change in size), appears to be valid, nor can glacial input be treated as ''normal'' steady state denudation products. However, given that the concentration is likely to be close to that representing the local denudation rate, it is safe to assume that partially glaciated catchments

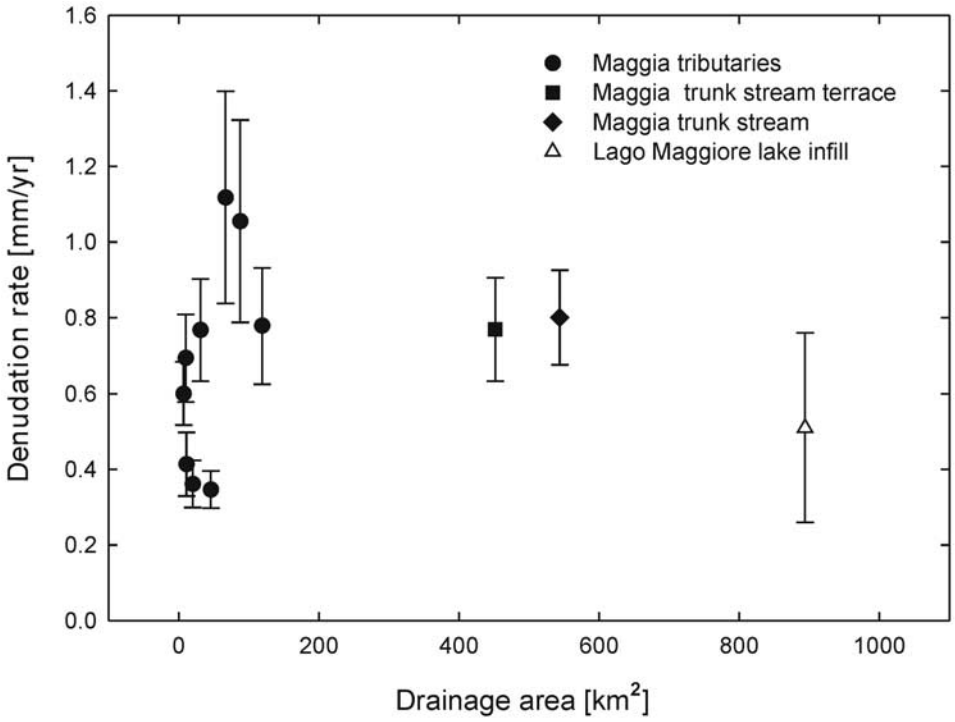

Figure 6. Cosmogenic nuclide-derived denudation rate (mm/a) versus drainage area (km^2) in the Maggia valley, southern Switzerland. Also plotted are the denudation rate for the Holocene terrace deposit (Mag 11-2) and the mechanical denudation rate for the Lago Maggiore derived from lake infill rates [taken from *Hinderer*, 2001].

can be measured with a minor additional error if the relative glaciated area is small (<10%). Denudation of moraine material can introduce a potential bias, especially if the time elapsed since the cessation of glaciation is short and if the moraine material is removed by fluvial undercutting rather than being eroded continuously from the exposed surface. The observed scatter in cosmogenic nuclide-derived denudation rates could well be due to this. In the Mittelland, however, measured nuclide concentrations are in the range of recent denudation products, which could imply that LGM moraines and other glacial deposits have, in terms of cosmogenic nuclides, become integral parts of the landscape since deglaciation at 15 ka, and that inheritance merely serves to mitigate a possible deficit introduced into slowly eroding catchments after a transient LGM perturbation.

3.2.3. Test of Appropriate Catchment Size

[34] Cosmogenic nuclide-derived denudation rates in the Maggia catchment (without Centovalli) range between 0.35 to 1.12 mm/a (see Figures 5 and 6). For catchments with areas <60 km^2 the average denudation rate is 0.53 ± 0.18 mm/a (n = 6). This corresponds to a scatter of 34%. For catchments with areas >50–60 km^2 denudation rates average at 0.90 ± 0.17 mm/a (n = 5). This corresponds to a scatter of 19%. This cutoff corresponds to the transition from second-order to third-order streams. The observed variations in denudation rate cannot be attributed to differences in lithology, since the Maggia valley is a catchment of relatively uniform lithology, featuring crystalline rocks only. Infrequent land slides or rockfalls within the Maggia catchment might possibly account for the more or less irregular distribution of denudation rates in the tributaries of the Maggia. Tributaries favoring large mass wasting events would experience higher denudation rates than those where no landslides occur, due to the incorporation of less irradiated material from greater depths. At small catchment scales, there is a small likelihood of experiencing landslides, but as the catchment area increases, landslide events are adequately represented. We can compare this finding to the modeling results of *Niemi et al.* [2005], who suggested that the spread of denudation rate data drops significantly once an appropriate spatial threshold is exceeded. For denudation rates typical of the Maggia area, *Niemi et al.* [2005] predicted 100–200 km^2 to be representative catchments. This is similar to our observation. Our results suggest that differences in denudation of tributaries may indeed be influenced by the catchment size, and that sampling for cosmogenic nuclide analysis should preferentially be made on a larger scale if an influence by mass wasting cannot be quantified.

[35] To account for the reworking of Quaternary sediments in the Maggia main valley which possibly yield different nuclide concentrations, we analyzed a sample from a river terrace in the main trunk stream of the Maggia at Riveo (Mag 11-2). This sample was amalgamated from a depth of ~1 m to ~3 m below the surface of the terrace and is thus representative of the material presently admixed into the trunk stream of the Maggia from fluvial deposits. The calculated denudation rate is 0.77 ± 0.14 mm/a. This result is identical within one σ error with the denudation rate acquired from the fluvial sediment denudation rate of the trunk stream at Moghegno (Mag 11-4), which is 0.80 ± 0.13 mm/a. Within error this is identical to the average of all tributaries, which is 0.73 ± 0.14 mm/a. These rates are also similar to denudation rates of 0.51 mm/a integrated since

LGM for lake fills in Lago Maggiore (see Table 3 and Figure 6) [*Hinderer*, 2001]. This adds confidence to the robustness of our approach.

[36] We conclude that the sampling of large, formerly glaciated valleys is a feasible approach and that in this environment, a catchment size in excess of 50 to 60 km^2 yields representative rates. We therefore applied this strategy to a north-south traverse of large catchments.

4. Denudation Rate Results and Basin Characteristics

4.1. Denudation Rates for the North-South Traverse

[37] In the high crystalline Alps, mean denudation rates are 0.9 ± 0.3 mm/a, where integration times are 0.5–1.5 ka, and 0.27 ± 0.14 mm/a for the Alpine foreland, where integration times are 1.9–8.4 ka. We begin with samples from southern Central Alps, followed by Valais and Central Alps samples and we will finish this section with presenting samples from the Swiss Mittelland. Samples "a" and "b" denote two different grain sizes of the same sample, "a" being the finer fraction. For nuclide concentrations see Table 2.

[38] The two southernmost samples are from the river Anza close to the Toce confluence, Valle Anzasca, Italy, and sample Sesia from the river Sesia at Varallo, Valle delle Sesia, Italy, respectively. Denudation rates are 0.83 ± 0.26 and 0.50 ± 0.09 mm/a, respectively. These two basins have many common characteristics, such as comparable mean altitudes, slopes, land use, climate, and rock uplift rate (see Tables 1 and S1), but with the southern slopes of Monte Rosa the Anza catchment contains a slightly larger fraction of glaciated landscape. In the catchment of the Maggia, we measured the trunk stream of the Maggia at Moghegno (sample Mag 11-4). This sample gives a denudation rate of 0.80 ± 0.13 mm/a. The trunk stream denudation rate agrees well with Maggia subcatchments larger than 60 km^2 (see Figure 5 and section 3.2.3). Furthermore, we measured sediment from the southern Central Alpine Toce and Verzasca (upstream of the Verzasca dam) catchments (samples Toce a and b, Verz a and b). The samples give the following denudation rates: Toce a 0.89 ± 0.15 mm/a; Toce b 1.46 ± 0.33 mm/a; Verz a 0.60 ± 0.11 mm/a and Verz b 0.59 ± 0.12 mm/a. These rates are all similar to those obtained in the neighboring Maggia valley.

[39] In the southern Central Alps, the catchment of the Melezza (Centovalli) was sampled in some detail (samples Mela 1, Mela 2, Mela 3a, and Mela 3b, respectively.) The "Mela" samples are all from the Centovalli, but are taken at different points within the valley. Mela 1 was taken ~11 km upstream of the Isorno-Melezza confluence at Dissimo, sample Mela 2 was taken at Intragna upstream of the Isorno-Melezza confluence, and samples Mela 3 a and b were taken ~1.5 km downstream of the confluence at Verscio, including Valle Onsernone, a small side valley of Centovalli (see Figure 1). The Centovalli samples give the following denudation rates: Mela 1 1.28 ± 0.26 mm/a; Mela 2 1.05 ± 0.39 mm/a; Mela 3a 0.66 ± 0.16 mm/a; Mela 3b 0.56 ± 0.10 mm/a. Field investigation showed that the upper part of the Centovalli near Dissimo is covered with thick late Quaternary glaciofluvial deposits, which yielded zero nuclide concentration when measured (see Section 3.2.2). Incorporation of these deposits by fluvial undercutting potentially explains the high denudation rates obtained for samples Mela 1 and Mela 2. Denudation rates decrease with increasing distance to late glacial deposits. As the influence of these sediments decreases downstream, nuclide concentrations are increasingly dominated by "normal" hillslope denudation products. These appear to dominate denudation rates at the Isorno-Melezza confluence. Since the Isorno catchment (Valle Onsernone) was not sampled separately, the mixing proportions beneath the confluence cannot be assessed. Since field inspections showed no evidence of glaciofluvial material in the Isorno catchment it can be assumed that this tributary introduces sediment with nuclide concentrations representative of the current hillslope erosion processes. All measured denudation rates of the Centovalli are all within the same range as the Maggia samples (see section 3.2.3). This indicates that the entrained nearly zero concentration material represents only a small fraction of the total sediment flux.

[40] In the Northern Valais, we sampled the valley of the river Lonza (Lötschental, sample Lonza). We also sampled the Milibach river, which is a tributary of the Rhône river southeast of Grengiols (sample Gren). Denudation rates are 1.28 ± .32 and 1.32 ± 0.43 mm/a, respectively. The Lonza valley is presently glaciated to a considerable extent (27%), the catchment of the Milibach on the other hand is presently nonglaciated, but features to some extent more readily erodible rocks. In the Central Alps, tributaries to the Rhône and Reuss rivers (samples Chie and Furka, respectively) and the trunk stream of the upper Ticino (sample Tic) were sampled. Chie and Furka yield denudation rates of 0.69 ± 0.17 and 1.14 ± 0.20 mm/a, respectively. The samples Tic a and Tic b yield denudation rates of 0.97 ± 0.23 and 0.63 ± 0.12 mm/a, respectively. Samples Reuss a and b are taken from the mainstream of the Reuss river, immediately upstream of the Vierwaldstättersee (Lake Lucerne) at Seedorf. Calculated denudation rates are 1.29 ± 0.38 and 1.87 ± 0.79 mm/a, respectively, and range among the highest measured in the Central Alps. A bias in denudation rate estimates due to glaciation cannot be ruled out for the high-Alpine catchments Chie, Furka, Lonza, and Reuss given their large areas currently glaciated (see Table S1, 23%, 21%, 27%, and 12% glaciated areas, respectively). However, the estimates are identical within error to nonglaciated catchments of otherwise similar basin characteristics like Tic and Gren.

[41] Catchments from the Swiss Mittelland all comprise Molasse sediments (sandstones, shales, and conglomerates). Samples from small, formerly unglaciated catchments (<25 km^2) are Bütsch 1 and 2 (river Bütschelbach), and samples from small catchments that were glaciated in LGM are Wasen 1-1 and 1-2 (river Liechtguetbach) and Taf (river Tafersbach). In these catchments of reduced relief, rockfalls and land slides are rare. Hence sampling of these catchments despite their small areas is legitimate. The cosmogenic nuclide-derived denudation rates are: 0.11 ± 0.02 and 0.1 ± 0.01 mm/a for Bütsch 1 and 2; 0.30 ± 0.07 and 0.28 ± 0.05 mm/a for Wasen 1-1 and 1-2; and 0.16 ± 0.02 mm/a for Taf. We see no dependence between nuclide concentration (see Table 2) and LGM ice cover. Samples from larger streams (>160 km^2) are Klem a and b (river Kleine Emme), Emme (river Emme), and Sense (river Sense). These three catchments were presumably partly glaciated in the LGM.

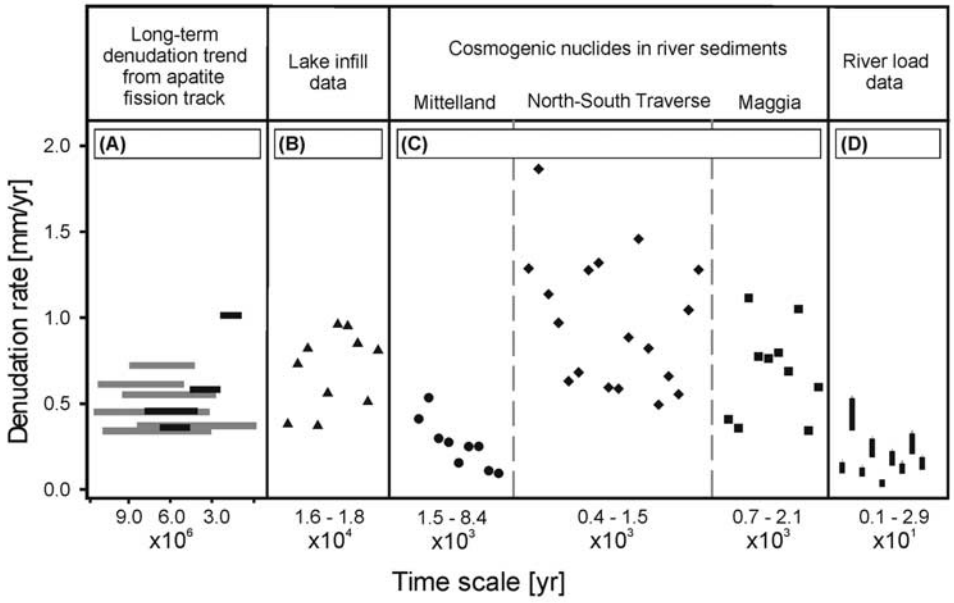

Figure 7. Denudation rate estimates from different methods plotted against their corresponding integration timescale (a); in the case of cosmogenic nuclide-derived denudation rates, this timescale corresponds to the apparent age. (a) Long-term denudation rate trends from apatite fission track data (black from *Wagner et al.* [1977]; gray from *Rahn* [2001, 2005]) plotted against apatite ages. Data from *Wagner et al.* [1977] have been recalculated to mean denudation rate values for each interval as explained in section 5.2. (b) Mechanical denudation rates from lake infill rates [from *Hinderer*, 2001]. (c) Summary of all measured cosmogenic nuclide-derived denudation rates from alluvial sediment samples, including Maggia tributaries. (d) Total denudation rates calculated from sedimentary river loads using a density of 2.5 g/cm^3 [from *Hinderer*, 2001], with positive error bars for a methodological error of 50%, because the chemical component of total denudation is not available for all samples. The chemical component is estimated to amount to ~50% on the basis of a compilation from the entire Alps (M. Hinderer, personal communication, 2006).

The respective denudation rates are: 0.42 ± 0.08 and 0.54 ± 0.13 mm/a for Klem a and b; 0.26 ± 0.03 mm/a for Emme; and 0.25 ± 0.05 mm/a for Sense. A detailed geomorphic analysis of formerly nonglaciated valleys of the Napf Area of the Mittelland has recently been performed by *Norton et al.* [2007]. There, cosmogenic nuclide-derived denudation rates are between 0.35 and 0.54 mm/a, where the faster rates are shown to be due to a transient, climate-related perturbation of the landscape.

4.2. Assessment of Grain Size Effects

[42] Nuclide concentrations from different quartz grain size fractions gave identical results within error limits for the samples Reuss, Verzasca, Mela 3, and Klem (Table 1). For the catchments of the Toce the larger fraction ("b," 800–1000 μm) yields a higher denudation rate (1.46 ± 0.33 mm/a) than the smaller fraction ("a," 250–500 μm, 0.89 ± 0.15 mm/a). This basin is very similar to that of the Verzasca, where both grain size fractions yield identical but lower denudation rates (~0.6 mm/a). In another Central Alpine catchment, the Ticino, the smaller fraction ("a," 125–250 μm) yields a higher denudation rate at 0.97 ± 0.23 mm/a than fraction "b" (250–500 μm with 0.63 ± 0.12 mm/a). It is difficult to attribute these discrepancies to certain basin characteristics, since overall catchments are similar. However, the percentage of area glaciated, the exact hillslope distribution, local gradients in precipitation and runoff, the distribution and frequency of rockfalls all differ slightly between catchments and could, potentially, introduce differences in nuclide concentrations between grain size fractions.

5. Discussion

5.1. Comparison With Denudation Rates From Lake Fills, River Gauging, and Fission Track Data

[43] We can now compare our catchment-wide cosmogenic nuclide-derived denudation rates (timescale 400–8400 a) with the rich database of other denudational monitors that operate over entirely different timescales. These are lake fills (timescale 10^4 a), river load gauging and delta growth (10–100 a), and fission track data (10^6 a; see Figure 7).

[44] Cosmogenic nuclide-derived denudation rates record both mechanical erosion and chemical weathering products, whereas lake infill rates only record mechanical erosion, thereby representing minimum estimates. In the Alps, lake fills integrate over an accumulation period since LGM and range between 0.5 and 1 mm/a for the high Alps (Table 3 and Figure 7). In view of the potential errors affecting both methods, an agreement to 30% between lake fill-derived rates and our cosmogenic nuclide-derived rates is excellent. Error estimates on lake infill rates by *Hinderer* [2001] include a stratigraphic error of ≤10% for Western Alpine

valleys; for the Southern Alps, this error might be as high as 50%. Adding an additional chemical component to lake fills would increase those rates and hence improve the agreement between methods. Other possibly introduced sources of error are (1) the conversion of sediment volumes into erosion rates because of the determination of bulk densities, and (2) the possible variation of glacial versus fluvial denudation with respect to our integration timescale. Despite these uncertainties, the agreement within 30% between post-LGM rates and cosmogenic rates might suggest that our new rates have been within this range since 15 ka.

[45] Delta growth rates record erosion rates and integrate over at the most the last 100 a. Delta growth rates are in general lower than cosmogenic nuclide-derived rates (Table 3); the reason for this discrepancy lies in integration timescale differences or is due to the absence of chemical weathering rates in delta growth rates.

[46] A similar picture arises from denudation rates from modern river loads based on suspended and dissolved loads, which vary between 0.3 and 0.36 mm/a [*Hinderer*, 2001]. Cosmogenic nuclide-derived denudation rates are consistently higher by a factor of 5–10 (Figure 7). This is a phenomenon that has been reported from nonorogenic settings [*Kirchner et al.*, 2001; *Schaller et al.*, 2001]. One possible explanation for this discrepancy is found in the systematic underestimation of denudation rates from sediment yield data [*Schaller et al.*, 2001], resulting from the short-term integration timescale of modern denudation rates, that does not record sediment discharged during rare flood events or temporarily stored on floodplains [*Summerfield*, 1991; *Summerfield and Hulton*, 1994; *Kirchner et al.*, 2001]. A second source of uncertainty of modern denudation rate estimates from river loads can be found in the contribution of bed load transport to the mechanical denudation rate. Cosmogenic nuclide-derived denudation rates on the other hand reflect long-term average rates of denudation that are independent of the present-day sediment flux [*Brown et al.*, 1995b, 1998; *Granger et al.*, 1996].

[47] The large discrepancy between modern and cosmogenic nuclide-derived denudation rates could also result from the overestimation of cosmogenic denudation rates with respect to modern rates of denudation. An overestimation could be caused by spatially nonuniform denudation due to linear dissection of a landscape. These types of sediment supply processes (see details on the effects of *Schaller et al.* [2001]; *von Blanckenburg et al.* [2004]) lead to preferential erosion of material having lower nuclide concentrations, resulting in higher denudation rates. For example, it has been suggested that within the Swiss Mittelland only 30% of the landscape is actively eroding by relief-forming fluvial dissection, whereas the remaining sections are maintaining their glacially sculpted morphology [*Schlunegger and Hinderer*, 2003]. It is also possible that parts of the landscape are not in cosmogenic steady state after being zeroed by glacial erosion in LGM (see section 3.2.1). This would result in a deficit in nuclide concentrations and hence in an overestimate of erosion rates. However, this effect would be most profound in areas of low denudation rate (Figure 3). Therefore we suggest that this process is less suited to explain our high cosmogenic denudation rates, which provide the largest difference to river load-based estimates.

[48] Finally, a possible factor influencing cosmogenic denudation rates might result from anthropogenic perturbations. Settlements in the Alps became more frequent at the beginning of Mesolithic Age (~10 ka ago), when woodland was being cleared to gain arable land. At the end of the early medieval times, this resulted in a depression of the forest boundary up to 300 m which was furthermore enhanced by climatic regressions [*Furrer et al.*, 1987]. Because of this long-term history of human settlement in the Alps, human activity could even have affected our long-term cosmogenic denudation rates. Recent anthropogenic disturbances include winter skiing, tourism, and road and tunnel construction. They should not have an effect on cosmogenic nuclide-derived denudation rates because of their long integration timescale [*von Blanckenburg*, 2005], but they might affect modern river loads. This also applies to the construction of dams in the high Alps, retaining a major part of the sediment in reservoir lakes. In any case the geomorphic activity of humans is less likely to affect denudation rates from cosmogenic nuclides, but other than dam construction, human activity would certainly increase modern river loads, resulting in an improved agreement between the two methods.

[49] Long-term denudation rate trends have been derived from apatite fission track cooling ages from vertical sections [*Wagner et al.*, 1977; *Rahn*, 2001, 2005]. We used this data set rather then spatially distributed apatite dates [e.g., *Rahn and Grasemann*, 1999], because *Wagner et al.* [1977] and *Rahn* [2001, 2005] have taken vertical age sections from which paleodenudation rates can be calculated without assumptions on geothermal gradients. However, it has to be acknowledged that age-elevation data from high-relief areas such as the Alps may provide overestimates of exhumation rates because of the topographic effect on age-elevation patterns [*Stuewe et al.*, 1994; *Braun*, 2002]. The long-term denudation rates from apatite ages are within the same order of magnitude as our cosmogenic nuclide-derived denudation rates (see Figure 7), but those measured for the period up to ~5 Ma ago are roughly half of the cosmogenic nuclide-based estimates. For the Gotthard Massif, uniform denudation rates of 0.6 mm/a for the last 10 Ma were determined. In the Ticino area, denudation rates within the period of 8–5 Ma ago have been constant at 0.4–0.3 mm/a. In the Monte Rosa region, an increase in denudation rates from 0.3 mm/a at 6 Ma to 0.7 mm/a at 3 Ma was recorded. In the Simplon-Antigorio area, a major increase in denudation from 0.5 to 0.9 mm/a at ~2.8 Ma took place, which was followed by a slight increase to 1.1 mm/a ~1.6 Ma ago [*Wagner et al.*, 1977]. *Rahn* [2001, 2005] has measured several traverses normal to the WSW-ENE Alpine strike, using mainly river valleys as natural incisions into the Alpine edifice. In the Rhône valley, a denudation rate of 0.6 mm/a for a period from 9.5 to 3.3 Ma ago was determined. Denudation rates along the Reuss valley in the Gotthard region were in the range of 0.5 mm/a 11.5–3.7 Ma ago. In the region of the Aar massif, a slightly higher denudation rate of 0.6 mm/a for the period 11.1–5.4 Ma was recorded. A traverse along the Rhine valley (Vättis window) for the period 8.5 Ma to today gives a mean denudation rate of 0.4 mm/a. Additional data along the upper Rhine valley (Glarus) yields a denudation rate of 0.7 mm/a for a period from 9 to 4.7 Ma BP [*Rahn*, 2001].

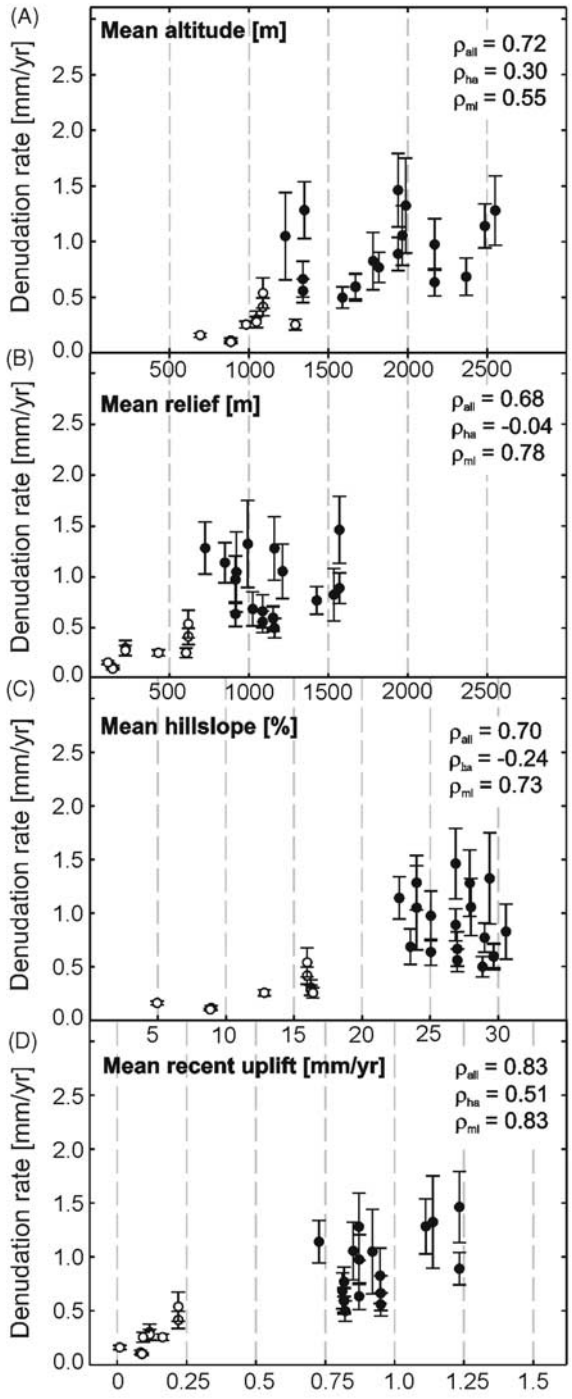

Figure 8. Comparison of (a) catchment-wide mean altitudes, (b) mean relief (calculated as mean altitude minus minimum altitude), (c) mean slope, and (d) recent rock uplift rates [from *Schlatter et al.*, 2005], with cosmogenic nuclide-derived denudation rates (mm/a) from Mittelland and high Alps alluvial sediment samples (Maggia trunk stream rates only). Open symbols are Mittelland samples, and solid symbols are high Alps samples. Also indicated are correlation coefficients ρ_{all} for all samples, ρ_{ha} for high-alpine samples only, and ρ_{ml} for Mittelland samples only. The error on scaling factor is not included for intersample comparison. Sample Reuss was omitted because of its large error.

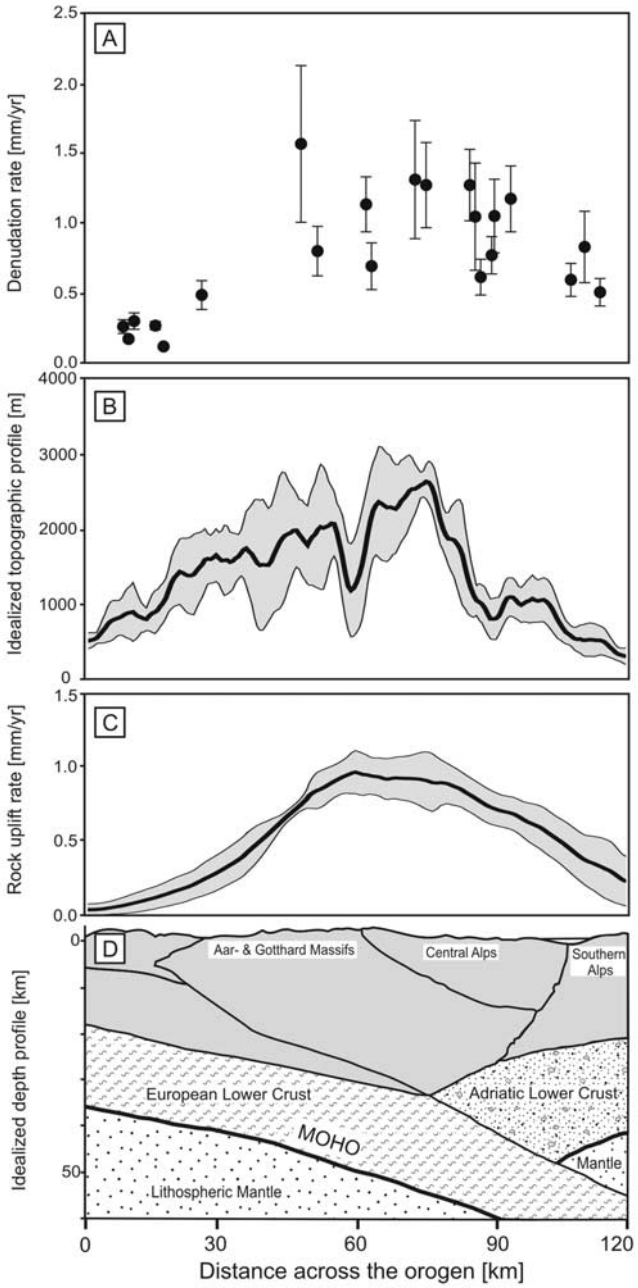

Figure 9. (a) Denudation rates measured with cosmogenic nuclides (Maggia trunk stream rates only). (b) Idealized topographic profile projected from several Alps-perpendicular profiles into a single plane. Range envelope is denoted as a swath with the width of the standard deviation of topography. (c) Idealized recent rock uplift pattern with range envelope also denoted as a standard deviation–wide swath [after *Schlatter et al.*, 2005]. (d) Idealized orogenic depth profile (simplified after *Schmid and Kissling* [2000] and *Schmid et al.* [2004]). All plots are plotted versus distance across the orogen (km). For catchments where two denudation rates were measured, a mean value was calculated.

Data from the Adula nappe indicate a long-term denudation rate of 0.35 mm/a within the period from 10.8–3.6 Ma [*Rahn*, 2005].

[50] Paleodenudation rates from careful sediment budgets of the entire Western and Swiss Alps by *Kuhlemann et al.* [2002] have reported denudation rates from 9–6 Ma of half the magnitude to those prevailing from 5 Ma to today. Therefore the evidence from cosmogenic nuclides and apatite fission track data appears to suggest that the modern denudation rates are a long-term feature that has been prevailing for the last few Ma, but that rates have roughly doubled in the last 5 Ma.

5.2. Constraints on Factors Controlling Denudation Rates

[51] A close inspection of Figure 2 appears to suggest that the spatial patterns of uplift correlate with spatial patterns of denudation. In Figure 8 we present a more detailed analysis of the correlation between topographic parameters with denudation rate. At first sight, correlations appear to exist between mean relief, mean altitude, mean slope, and mean recent uplift rate on the one hand and spatially averaged denudation rate on the other hand. Correlation coefficients are all >0.7 (Figure 8). The geographic trend shown in Figure 9 seems to suggest that denudation rates are highest where mean altitude, rock uplift rate, and crustal thickness are greatest. These maxima are all focused around the centre of the orogen. A more detailed look however reveals that our data are also compatible with a representation in terms of two distinct sample groups: Mittelland catchments have low denudation rates (0.1–0.5 mm/a) and also low relief, low mean altitude, low hillslope gradients, and low recent uplift rate, while the high-Alps catchments are characterized by high denudation rates (0.5–1.3 mm/a; omitting sample Reuss because of its high analytical error), and also high relief, high mean altitude, high hillslope gradients, and high recent uplift rate. Interestingly, the Mittelland samples show good correlations with these four topographic parameters. Correlation coefficients are between 0.6 and 0.8. We interpret the morphology of the Mittelland in terms of a landscape that is actively adjusting to recent change. Such change can be an external forcing such as tectonic change, or major climate change. For example, the adjustment of the landscape after having been overridden by the large relief-sculpting LGM glaciers might represent such a transient situation, or, alternatively, changes in uplift rate relative to a local base level. As a result, the landscape reacts with high sensitivity to parameters that might ultimately result in high spatial denudation. Governing factors such as drainage network reorganization have been documented by *Schlunegger et al.* [2001]. The situation of the high Alps is different. Neither mean relief, nor altitude, nor hillslope appears to correlate with denudation rates. A weak correlation is visible between recent uplift rate and denudation rate ($r = 0.51$). One possibility for the absence of such correlations has been pointed out by *Montgomery and Brandon* [2002]. In catchments of high denudation rates rivers incise at a rate that is so high that hillslopes react with mass wasting. In this case the relief or slopes are limited to a certain threshold value that is governed by the rock strength. Consequently, the denudation rate is independent of these parameters. On the basis of our data for the high Alps, this threshold relief is possibly reached at ~800 m, while the threshold slope is ~22% (see Figure 8).

5.3. Are Denudation and Rock Uplift Rates in Equilibrium?

[52] Least squares regression [*Ludwig*, 1994] of our cosmogenic nuclide-derived denudation rates for the high Alps against the uplift data from *Schlatter et al.* [2005] yields a slope of 1.0 ± 0.25, where the uncertainty represents the 95% confidence limits on the best fit line with an intercept at the origin at 0 ± 0.2. We omit sample Reuss because of its high error (see Figure 8). Several scenarios are conceivable that might generate the agreement between denudation rates and rock uplift rates.

[53] At tectonic steady state, rock uplift equals denudation. It has been argued by *Whipple* [2001] that this form of equilibrium can prevail even if the long-term steady state has been perturbed, as it is likely in the Alps because of late Quaternary climate change represented by the deglaciation at 15–10 ka. When a small change in convergence rate or erosional efficiency (e.g., a climate change) introduces a perturbation, both rock uplift and denudation are perturbed. However, with a small lag time that depends on the nature of the change, they will agree with each other despite being in the transient phase of readjustment [*Whipple and Meade*, 2006]. Therefore denudation and rock uplift can agree with each other even if the orogen is in a transient phase. In a second scenario, we assume that the long-term rock uplift in the Alps is in steady state and equals an average denudation rate, but this average denudation rate in reality displays small, possibly climate-caused variations. If the amplitude of these variations is small, it might be contained within the scatter of our denudation rate data, and in any case might be damped by the method integration time. A variant of the second scenario is that the changes in denudation rates caused by glacial cycles are strongly focused in local areas (e.g., glacial valleys), and thus, although there the rates may be significantly higher, they do not strongly influence our catchment-wide denudation rates. In a third model the recent uplift pattern is explained by postglacial isostatic rebound after major glaciations due to melting of ice caps [*Gudmundsson*, 1994] or melting of recent glaciers following the Little Ice Age [*Barletta et al.*, 2006]. While this view was challenged by *Persaud and Pfiffner* [2004], it is difficult to conceive, however, why denudation should agree with rock uplift if the timescale for rock uplift is so short. For increased rock uplift to result in increased denudation rates, the extensive migration of knickpoints and the propagation of the adjusted river network into the entire landscape are required. We consider it very questionable whether such an adjustment can have taken place in a period as short as 15 ka, not to mention the few hundred years since the Little Ice Age. A fourth model assumes crustal thickening due to orogenic convergence at any time in the past since the onset of convergence, where relief is isostatically balancing the thickness of the crust. Changes in precipitation, temperature, and glacial activity pattern enhance denudation [*Kuhlemann et al.*, 2002], which would then drive rock uplift due to isostatic compensation [*Stuewe and Barr*, 1998; *Zhang et al.*, 2001; *Bernet et al.*, 2004; *Champagnac et al.*, 2007].

[54] The postglacial rebound models agree with the assumption that the Alps are more or less "dead," e.g., that no active convergence drives isostatic compensation [*Molnar*, 2004]. Other workers, however, [e.g., *Dezes et al.*, 2004] hold the view that the tectonic convergence in the Alps is currently still active. On the basis of an estimation of mean rock uplift for the Central Alps [*Schlatter et al.*, 2005], we can calculate an approximated convergence rate of the orogen via equation (6),

$$V_A = \frac{U^*W}{D_W} \tag{6}$$

where V_A is the convergence rate of the orogen (mm/a), U is the mean rock uplift (~0.6 mm/a), W is the width of the orogen (~100 km), and D_W is the depth of the orogenic wedge (~30 km). We obtain a mean orogenic convergence rate of ~2 mm/a, which is in the range of residual velocities with respect to stable Europe measured in the Western Alps by *Calais et al.* [2002]. However, *Delacou et al.* [2004] argue that no direct effect of Europe/Africa convergence can be identified and that the main features of the current stress field in the Alps is due to extension in the inner areas of the belt and zones of compression at the outer boundaries. So far no conclusive evidence for convergence in the Central Alps can be used to explain the patterns of uplift and denudation.

[55] In the light of this evidence, we can speculate about the timescale of the steady state between rock uplift and denudation rates. Sediment balances suggest a strong increase in denudation in the last 5 Ma [*Kuhlemann et al.*, 2002]. Regardless of the causes for this increase, *Willett et al.* [2006] suggested that this change in erosional mass flux led to a decrease in size of the active wedge, causing the thrust fronts to retreat toward the centre of the orogen, which then led to a focus of deformation into the wedge interior, or a contraction of the overall active orogen. In a similar approach, *Cederbom et al.* [2004] suggested that the observed change in mass flux caused isostatic exhumation of the high Central Alps while flexural rebound occurred in the Molasse foreland basin. Our observation of two sample groups is consistent with both models. We suggest that our two distinct sample groups (Figure 8) represent the rather low rock uplift rates in the Mittelland, being equal to our cosmogenic nuclide-derived denudation rates, and the rather high rock uplift rates in the high Alps, which accordingly are due to active convergence tectonics, correspond to higher denudation rates. It is well possible that these uplift-denudation patterns are features that have been prevailing for at least a few million years, as has also been suggested by *Bernet et al.* [2004].

[56] In support of this, it is observed that spatial geodetic uplift rate patterns are roughly identical to spatial patterns of apatite fission track ages for the period between 2 and 10 Ma [*Persaud and Pfiffner*, 2004], an observation that was also made for the Eastern Alps [*Frisch et al.*, 2000]. 3 Ma ago is the time when apatite fission track-derived denudation rates from the Simplon area [*Wagner et al.*, 1977] moved into the range reflected by our cosmogenic nuclide-derived rates (Figure 7), although it has to be acknowledged that the Simplon data record the highest long-term denudation rates and are somewhat geographically offset from our set of data. For the Central and Western Alps, denudation rate increases were recorded at ~5 Ma ago from sediment budgets [*Kuhlemann et al.*, 2002]. All this evidence is not incompatible with our rates showing long-term steady state denudation, although the other hypotheses discussed above cannot be discounted either.

6. Conclusions

[57] Mean denudation rates measured by cosmogenic ^{10}Be in river sediment are 0.27 ± 0.14 mm/a for the Alpine foreland, where integration times are 1.9–8.4 ka, and 0.9 ± 0.3 mm/a for the high crystalline Alps, where integration times are 0.4–1.5 ka. Basin-averaged hillslope angles are independent of denudation rate in the high Alps and are limited to 25–30%. In the Mittelland, denudation rates correlate with hillslope angle as well as with relief and uplift rate. This might suggest that the Swiss Alps region with its Molasse foreland basin comprises two distinct domains: the high Central Alps accommodate most of the uplift and denudation that possibly contains a component of isostatic rebound or convergence-driven uplift, while the Mittelland has been decoupled from this active regime.

[58] The most important observation made is the correlation between cosmogenic nuclide-derived denudation rate and rock uplift rate. Both these parameters are highest where altitude, relief, and crustal thickness are highest. This might indicate some form of steady state between uplift and denudation. Such a finding is surprising given that the Alps are only just recovering from the major perturbation represented by the melting of thick LGM glaciers. One possibility is that although steady state after these events has not been established, variations in erosional efficiency caused by climate change or changes in uplift rate caused by postglacial rebound mimic each other with a short lag time, making the two indistinguishable. A second explanation is that the amplitude of glacial/interglacial denudation rate changes is not as large as it might intuitively be expected and is contained in the scatter of our rates (~30%). A third explanation is that the recent uplift pattern is explained by postglacial isostatic rebound after major glaciations due to melting of ice caps or melting of recent glaciers following the Little Ice Age but if true the mechanism at which denudation rates adjust at the same level as uplift is not obvious. Fourth, changes in precipitation, temperature, climate cycling, and glacial activity after ~5–3 Ma ago might have enhanced denudation, which would then simply drive rock uplift due to isostatic compensation. Finally, it might well be that at present convergence and accretionary flux set the pace of both rock uplift and denudation of the high Central Alps, but to date no conclusive evidence exists that such convergence is still active. The agreement between denudation rates determined over the 10^2, 10^4, and 10^6 a timescale appears to lend some support to the suggestion that some large-scale form of denudational steady state might be a long-term feature for the Central Alps.

[59] **Acknowledgments.** We are grateful to Meredith Kelly, Alfons Berger, and Ronny Schoenberg for support during sampling campaigns and advice; Christian Schlüchter for advice on glacial histories; Veerle Vanacker for numerous discussions and the implementation of a skyline shielding algorithm; and discussions with Fritz Schlunegger, Joachim Kuhlemann,

Matthias Hinderer, and Ralf Hetzel. We also thank Andreas Schlatter from the Bundesamt für Landestopographie, Switzerland, for providing rock uplift data and Christoph Marty from SLF, Davos, for providing snow distribution data. Lesley Perg is acknowledged for sample preparation of glacial sediment and Mittelland samples. This manuscript was greatly improved by the careful and constructive reviews by Peter van der Beek, an anonymous reviewer, and associate editor Alex Densmore. This work was funded by DFG grant Bl 562-2.

References

Auer, M. (2003), Regionalisierung von Schneeparametern—Eine Methode zur Darstellung von Schneeparametern im Relief, M.S. thesis, 97 pp., Univ. Bern, Bern.

Barletta, V. R., C. Ferrari, G. Diolaiuti, T. Carnielli, R. Sabadini, and C. Smiraglia (2006), Glacier shrinkage and modeled uplift of the Alps, *Geophys. Res. Lett.*, *33*, L14307, doi:10.1029/2006GL026490.

Bernet, M., M. Brandon, J. Garver, and B. Molitor (2004), Downstream changes of Alpine zircon fission-track ages in the Rhone and Rhine rivers, *J. Sediment. Res.*, *74*, 82–94.

Bierman, P., and K. Nichols (2004), Rock to sediment—Slope to sea with ^{10}Be—Rates of landscape change, *Annu. Rev. Earth Planet. Sci.*, *32*, 215–255.

Bierman, P., and E. Steig (1996), Estimating rates of denudation using cosmogenic isotope abundances in sediment, *Earth Surf. Processes Landforms*, *21*, 135–139.

Brandon, M., and J. Vance (1992), Tectonic evolution of the Cenozoic Olympic subduction complex, Washington State, as deduced from fission track ages for detrital zircons, *Am. J. Sci.*, *292*, 565–636.

Braun, J. (2002), Quantifying the effect of recent relief changes on age-elevation relationships, *Earth Planet. Sci. Lett.*, *200*, 331–343.

Brown, E. T., D. L. Bourlès, F. Colin, G. M. Raisbeck, F. Yiou, and S. Desgarceaux (1995a), Evidence for muon-induced production of ^{10}Be in near-surface rocks from the Congo, *Geophys. Res. Lett.*, *22*, 703–706.

Brown, E. T., R. Stallard, M. Larsen, G. Raisbeck, and F. Yiou (1995b), Denudation rates determined from the accumulation of in situ- produced ^{10}Be in the Luquillo experimental forest, Puerto Rico, *Earth Planet. Sci. Lett.*, *129*, 193–202.

Brown, E. T., R. Stallard, M. Larsen, D. Bourles, G. Raisbeck, and F. Yiou (1998), Determination of predevelopment denudation rates of an agricultural watershed (Cayaguas River, Puerto Rico) using in-situ-produced ^{10}Be in river-borne quartz, *Earth Planet. Sci. Lett.*, *160*, 723–728.

Calais, E., J. Nocquet, F. Jouanne, and M. Tardy (2002), Current strain regime in the Western Alps from continuous Global Positioning System measurements, 1996–2001, *Geology*, *30*, 651–654.

Cederbom, C., H. Sinclair, F. Schlunegger, and M. Rahn (2004), Climate-induced rebound and exhumation of the European Alps, *Geology*, *32*, 709–712.

Champagnac, J., P. Molnar, R. Anderson, C. Sue, and B. Delacou (2007), Quaternary erosion- induced isostatic rebound in the western Alps, *Geology*, *35*, 195–198.

Delacou, B., C. Sue, J. Champagnac, and M. Burkhard (2004), Present-day geodynamics in the bend of the Western and Central Alps as constrained by earthquake analysis, *Geophys. J. Int.*, *158*, 753–774.

Dezes, P., S. Schmid, and P. Ziegler (2004), Evolution of the European Cenozoic rift system: Interaction of the Alpine and Pyrenean orogens with their foreland lithosphere, *Tectonophysics*, *389*, 1–33.

Dunai, T. (2000), Scaling factors for production rates of in situ produced cosmogenic nuclides: A critical reevaluation, *Earth Planet. Sci. Lett.*, *176*, 157–169.

Dunne, J., D. Elmore, and P. Muzikar (1999), Scaling factors for the rates of production of cosmogenic nuclides for geometric shielding and attenuation at depth on sloped surfaces, *Geomorphology*, *27*, 3–11.

England, P., and P. Molnar (1990), Surface uplift, uplift of rocks, and exhumation of rocks, *Geology*, *18*, 1173–1177.

Florineth, D., and C. Schluechter (1998), Reconstructing the Last Glacial Maximum (LGM) ice surface geometry and flowlines in the Central Swiss Alps, *Eclogae Geol. Helv.*, *91*, 391–407.

Florineth, D., and C. Schluechter (2000), Alpine evidence for atmospheric circulation patterns in Europe during the Last Glacial Maximum, *Quat. Res.*, *54*, 295–308.

Frisch, W., B. Székely, J. Kuhlemann, and I. Dunkl (2000), Geomorphological evolution of the Eastern Alps in response to Miocene tectonics, *Z. Geomorphol.*, *44*, 103–138.

Furrer, G., C. Burga, M. Gamper, H. Holzhauser, and M. Maisch (1987), Zur Gletscher- Vegetations- und Klimageschichte der Schweiz seit der Spaeteiszeit, *Geogr. Helv.*, *2*, 61–91.

Granger, D. E., J. W. Kirchner, and R. C. Finkel (1996), Spatially averaged long-term erosion rates measured from in situ-produced cosmogenic nuclides in alluvial sediment, *J. Geol.*, *104*, 249–257.

Gudmundsson, G. (1994), An order-of-magnitude estimate of the current uplift-rates in Switzerland caused by the Wuerm Alpine deglaciation, *Eclogae Geol. Helv.*, *87*, 545–557.

Heidbreder, E., K. Pinkau, C. Reppin, and V. Schoenfelder (1971), Measurements of distribution in energy and angle of high-energy neutrons in lower atmosphere, *J. Geophys. Res.*, *76*, 2905–2916.

Hinderer, M. (2001), Late Quaternary denudation of the Alps, valley and lake fillings and modern river loads, *Geodin. Acta*, *14*, 231–263.

Hormes, A., B. U. Mueller, and C. Schluechter (2001), The Alps with little ice: Evidence for eight Holocene phases of reduced glacier extent in the Central Swiss Alps, *Holocene*, *11*(3), 255–265.

Hovius, N., and F. von Blanckenburg (2007), Constraining the denudational response to faulting, in *The Dynamics of Fault Zones*, edited by M. Handy, D. D. Hirth, and N. Hovius, chap. 9, pp. 231–273, MIT Press, Cambridge, Mass.

Hovius, N., C. Stark, C. Hao-Tsu, and L. Jiun-Chuan (2000), Supply and removal of sediment in a landslide-dominated mountain belt: Central Range, Taiwan, *J. Geol.*, *108*, 73–89.

Ivy-Ochs, S., C. Schluechter, P. Kubik, H. Synal, J. Beer, and H. Kerschner (1996), The exposure age of an Egesen moraine at Julier Pass, Switzerland, measured with the cosmogenic radionuclides ^{10}Be, ^{26}Al and ^{36}Cl, *Eclogae Geol. Helv.*, *89*, 1049–1063.

Ivy-Ochs, S., J. Schaefer, P. Kubik, H. Synal, and C. Schluechter (2004), Timing of deglaciation on the northern Alpine foreland (Switzerland), *Eclogae Geol. Helv.*, *97*, 47–55.

Jäckli, A. (1970), Die Schweiz zur letzten Eiszeit, Atlas der Schweiz, map 6, Eidg. Landestopogr. Wabern, Bern.

Kahle, H., et al. (1997), Recent crustal movements, geoid and density distribution: Contribution from integrated satellite and terrestrial measurements, in *Results of the National Research Program 20 (NRP 20)*, edited by O. E. A. Pfiffner, pp. 251–259, Birkhaeuser, Basel, Switzerland.

Kelly, M., J. Buoncristiani, and C. Schluechter (2004), A reconstruction of the Last Glacial Maximum (LGM) ice-surface geometry in the western Swiss Alps and contiguous Alpine regions in Italy and France, *Eclogae Geol. Helv.*, *97*, 57–75.

Kerschner, H., G. Kaser, and R. Sailer (2000), Alpine Younger Dryas glaciers as paleo-precipitation gauges, *Ann. Glaciol.*, *31*, 80–84.

Kerschner, H., A. Hertl, G. Gross, S. Ivy-Ochs, and P. W. Kubik (2006), Surface exposure dating of moraines in the Kromer valley (Silvretta Mountains, Austria)—Evidence for glacial response to the 8.2 ka event in the Eastern Alps?, *Holocene*, *16*, 7–15.

Kirchner, J. W., R. C. Finkel, C. S. Riebe, D. E. Granger, J. Clayton, J. King, and W. Megahan (2001), Mountain erosion over 10 yr, 10 k.y., and 10 m.y. time scales, *Geology*, *29*, 591–594.

Koons, P. (1989), The topographic evolution of collisional mountain belts: a numerical look at the Southern Alps, New Zealand, *Am. J. Sci.*, *289*, 1041–1069.

Kuhlemann, J., W. Frisch, B. Szekely, I. Dunkl, and M. Kazmer (2002), Post-collisional sediment budget history of the Alps: Tectonic versus climatic control, *Int. J. Earth Sci.*, *91*, 818–837.

Lal, D. (1991), Cosmic ray labeling of erosion surfaces: In situ nuclide production rates and erosion models, *Earth Planet. Sci. Lett.*, *104*, 424–439.

Lal, D., and B. Peters (1967), Cosmic ray-produced radioactivity on the Earth, in *Handbuch der Physik*, edited by S. Fluegge, pp. 551–612, Springer, Berlin.

Ludwig, K. R. (1994), ISOPLOT—A plotting and regression program for radiogenic isotope data, *U.S. Geol. Surv. Open File Rep. 91-445*, 45 pp.

Maisch, M. (1981), Glazialmorphologische und gletschergeschichtliche Untersuchungen im Gebiet zwischen Landwasser- und Albulatal (Kt. Graubünden, Schweiz), *Geogr. Helv.*, *37*, 93–104.

Masarik, J., M. Frank, J. Schaefer, and R. Wieler (2001), Correction of in situ cosmogenic nuclide production rates for geomagnetic field variations during the past 800,000 years, *Geochim. Cosmochim. Acta*, *65*, 2995–3003.

Molnar, P. (2004), Late Cenozoic increase in accumulation rates of terrestrial sediment: How might climate change have affected erosion rates?, *Annu. Rev. Earth Planet. Sci.*, *32*, 67–89.

Montgomery, D., and M. Brandon (2002), Topographic controls on erosion rates in tectonically active mountain ranges, *Earth Planet. Sci. Lett.*, *201*, 481–489.

Montgomery, D., and H. Greenberg (2000), Local relief and the height of Mount Olympus, *Earth Surf. Processes Landforms*, *25*, 385–396.

Mulch, A., C. Teyssier, M. A. Cosca, and C. P. Chamberlain (2007), Stable isotope paleoaltimetry of Eocene core complexes in the North American Cordillera, *Tectonics*, *26*, TC4001, doi:10.1029/2006TC001995.

Niemi, N., M. Oskin, D. Burbank, A. Heimsath, and E. Gabet (2005), Effects of bedrock landslides on cosmogenically determined erosion rates, *Earth Planet. Sci. Lett.*, *237*, 480–498.

Norton, K. P., F. von Blanckenburg, F. Schlunegger, and P. W. Kubik (2007), Cosmogenic nuclide-based investigation of spatial erosion and

hillslope coupling in the geomorphically transient foreland of the Swiss Alps, *Geomorphology*, in press.
Ohlendorf, C. (1998), High alpine lake sediments as chronicles for regional glacier and climate history in the Upper Engadine, southeastern Switzerland, Ph.D. thesis, 203 pp., ETH Zurich, Zurich, Switzerland.
Parker, G., and L. Perg (2005), Probabilistic formulation of conservation of cosmogenic nuclides: Effect of surface elevation fluctuations on approach to steady state, *Earth Surf. Processes Landforms*, *30*, 1127–1144.
Persaud, M., and O. Pfiffner (2004), Active deformation in the eastern Swiss Alps: Post-glacial faults, seismicity and surface uplift, *Tectonophysics*, *385*, 59–84.
Pinet, P., and M. Souriau (1988), Continental erosion and large-scale relief, *Tectonics*, *7*, 563–582.
Prosser, G. (1998), Strike-slip movements and thrusting along a transpressive fault zone: The North Giudicarie line (Insubric line, northern Italy), *Tectonics*, *17*, 921–937.
Rahn, M. (2001), The metamorphic and exhumation history of the Helvetic Alps, Switzerland, as revealed by apatite and zircon fission tracks, habilitation thesis, 140 pp., Albert Ludwigs Univ. Freiburg, Freiburg, Germany.
Rahn, M. (2005), Apatite fission track ages from the Adula nappe: Late-stage exhumation and relief evolution, *Schweiz. Mineral. Petrogr. Mitt.*, *85*, 233–245.
Rahn, M., and B. Grasemann (1999), Fission track and numerical thermal modeling of differential exhumation of the Glarus thrust plane (Switzerland), *Earth Planet. Sci. Lett.*, *169*, 245–259.
Riebe, C. S., J. W. Kirchner, and D. E. Granger (2001), Quantifying quartz enrichment and its consequences for cosmogenic measurements of erosion rates from alluvial sediment and regolith, *Geomorphology*, *40*, 15–19.
Roebber, P., S. Bruening, D. Schultz, and J. Cortinas Jr. (2003), Improving snowfall forecasting by diagnosing snow density, *Weather Forecasting*, *18*, 264–287.
Roethlisberger, F., and W. Schneebeli (1979), Genesis of lateral moraine complexes, demonstrated by fossil soils and trunks; indicators of post-glacial climatic fluctuations, paper presented at INQUA Symposium on Genesis and Lithology of Quaternary Deposits, Int. Union for Quat. Res., Zurich, Switzerland.
Sailer, R. (2001), Spaeteiszeitliche Gletscherstaende in der Fernwallgruppe, Ph.D. thesis, 204 pp., Univ. Innsbruck, Innsbruck, Austria.
Schaller, M., F. von Blanckenburg, N. Hovius, and P. Kubik (2001), Large-scale erosion rates from in situ-produced cosmogenic nuclides in European river sediments, *Earth Planet. Sci. Lett.*, *188*, 441–458.
Schaller, M., F. von Blanckenburg, A. Veldkamp, L. Tebbens, N. Hovius, and P. Kubik (2002), A 30 000 yr record of erosion rates from cosmogenic ^{10}Be in middle European river terraces, *Earth Planet. Sci. Lett.*, *204*, 307–320.
Schildgen, T., W. Phillips, and R. Purves (2005), Simulation of snow shielding corrections for cosmogenic nuclide surface exposure studies, *Geomorphology*, *64*, 67–85.
Schlatter, A., D. Schneider, A. Geiger, and H. Kahle (2005), Recent vertical movements from precise levelling in the vicinity of the city of Basel, Switzerland, *Int. J. Earth Sci.*, *94*, 507–514.
Schlunegger, F., and M. Hinderer (2001), Crustal uplift in the Alps: Why the drainage pattern matters, *Terra Nova*, *13*, 425–432.
Schlunegger, F., and M. Hinderer (2003), Pleistocene/Holocene climate change, re-establishment of fluvial drainage network and increase in relief in the Swiss Alps, *Terra Nova*, *15*, 88–95.
Schlunegger, F., J. Melzer, and G. Tucker (2001), Climate, exposed source-rock lithologies, crustal uplift and surface erosion: A theoretical analysis calibrated with data from the Alps/north Alpine foreland basin system, *Int. J. Earth Sci.*, *90*, 484–499.
Schmid, S., and E. Kissling (2000), The arc of the western Alps in the light of geophysical data on deep crustal structure, *Tectonics*, *19*, 62–85.
Schmid, S., H. Aebli, F. Heller, and A. Zingg (1989), The role of the Periadriatic line in the tectonic evolution of the Alps, in *Alpine Tectonics*, edited by M. Coward, D. Dietrich, and R. Park, *Geol. Soc. Spec. Publ.*, *45*, 153–171.
Schmid, S., B. Fuegenschuh, E. Kissling, and R. Schuster (2004), Tectonic map and overall architecture of the Alpine orogen, *Eclogae Geol. Helv.*, *97*, 93–117.
Small, E., R. Anderson, J. Repka, and R. Finkel (1997), Erosion rates of alpine bedrock summit surfaces deduced from in situ ^{10}Be and ^{26}Al, *Earth Planet. Sci. Lett.*, *150*, 413–425.
Stuewe, K., and T. Barr (1998), On uplift and exhumation during convergence, *Tectonics*, *17*, 80–88.
Stuewe, K., L. White, and R. Brown (1994), The influence of eroding topography on steady-state isotherms: Application to fission track analysis, *Earth Planet. Sci. Lett.*, *124*, 63–74.
Summerfield, M. (1991), Tectonic geomorphology, *Prog. Phys. Geogr.*, *15*, 193–205.
Summerfield, M., and N. Hulton (1994), Natural controls of fluvial denudation rates in major world drainage basins, *J. Geophys. Res.*, *99*, 871–883.
Synal, H., G. Bonani, M. Doebeli, R. Ender, P. Gartenmann, P. W. Kubik, C. Schnabel, and M. Suter (1997), Status report of the PSI/ETH AMS facility, *Nucl. Instrum. Methods Phys. Res., Sect. B*, *123*, 62–68.
van Husen, D. (1977), *Zur Fazies und Stratigraphie der Jungpleistaozänen Ablagerungen im Trauntal (mit Quartärgeologischer Karte)*, *Jahrbuch Geol. Bundesanst.*, vol. 120, pp. 1–130, Verl. Geol. Bundesanst., Vienna.
Vezolli, G. (2004), Erosion in the Western Alps (Dora Baltea basin): 2. Quantifying sediment yield, *Sediment. Geol.*, *171*, 247–259.
von Blanckenburg, F. (2005), The control mechanisms of erosion and weathering at basin scale from cosmogenic nuclides in river sediment, *Earth Planet. Sci. Lett.*, *237*, 462–479.
von Blanckenburg, F., N. Belshaw, and R. O'Nions (1996), Separation of ^{9}Be and cosmogenic ^{10}Be from environmental materials and SIMS isotope dilution analysis, *Chem. Geol.*, *129*, 93–99.
von Blanckenburg, F., T. Hewawasam, and P. W. Kubik (2004), Cosmogenic nuclide evidence for low weathering and denudation in the wet, tropical highlands of Sri Lanka, *J. Geophys. Res.*, *109*, F03008, doi:10.1029/2003JF000049.
Wagner, G., G. Reimer, and E. Jaeger (1977), Cooling ages derived by apatite fission-track, mica Rb-Sr and K-Ar dating: The uplift and cooling history of the Central Alps, *Mem. Ist. Geol. Miner. Univ. Padova*, *30*, 1–27.
Ware, E., D. Schultz, H. Brooks, P. Roebber, and S. Bruening (2006), Improving snowfall forecasting by accounting for the climatological variability of snow density, *Weather Forecasting*, *21*, 94–103.
Whipple, K. (2001), Fluvial landscape response time: How plausible is steady-state denudation?, *Am. J. Sci.*, *301*, 313–325.
Whipple, K. (2004), Bedrock rivers and the geomorphology of active orogens, *Annu. Rev. Earth Planet. Sci.*, *32*, 151–185.
Whipple, K., and B. Meade (2006), Orogen response to changes in climatic and tectonic forcing, *Earth Planet. Sci. Lett.*, *243*, 218–228.
Whipple, K., E. Kirby, and S. Brocklehurst (1999), Geomorphic limits to climate-induced increases in topographic relief, *Nature*, *401*, 39–43.
Willett, S., and M. Brandon (2002), On steady states in mountain belts, *Geology*, *30*, 175–178.
Willett, S., F. Schlunegger, and V. Picotti (2006), Messinian climate change and erosionale destruction of the Central European Alps, *Geology*, *34*, 613–616.
Zhang, P., P. Molnar, and W. Downs (2001), Increased sedimentation rates and grain sizes 2–4 Myr ago due to the influence of climate change on erosion rates, *Nature*, *410*, 891–897.

T. Kruesmann, GFZ Potsdam, Telegrafenberg, Haus B, D-14473 Potsdam, Germany.
P. W. Kubik, Paul Scherrer Institut and Institute of Particle Physics, ETH Zurich, CH-8093 Zürich, Switzerland.
K. P. Norton, F. von Blanckenburg, and H. Wittmann, Institut für Mineralogie, Universität Hannover, Callinstr. 3, D-30167 Hannover, Germany. (h.wittmann@mineralogie.uni-hannover.de)